Theoretical Study of Structure and Spectra of Cage Clusters $(H_2O)_n$, $n = 7-10$

Joanna Sadlej

Department of Chemistry, University of Warsaw, Pasteura 1, 02-093 Warsaw, Poland and Drug Institute, Chelmska 30/34, 00-725 Warsaw, Poland

Victoria Buch*

The Fritz Haber Institute for Molecular Dynamics, Hebrew University, Jerusalem, 91904, Israel

J. K. Kazimirski

Industrial Chemistry Research Institute, Warsaw, Poland

Udo Buck

Max-Planck-Institut für Strömungsforschung, D-37073 Göttingen, Germany

Received: February 15, 1999; In Final Form: April 14, 1999

The optimal structures, interaction energies, and OH stretch frequencies of water cage clusters, $(H_2O)_n$, $n = 7-10$, have been investigated theoretically. The study consisted of MP2 level ab initio calculations of optimal structures and spectra and similar calculations employing an empirical polarizable potential. The study focuses predominantly on structures, that were used for assignment of recently measured size selected OH stretch spectra. The structures are related to octamer cubes. The nonamer and the decamer are derived from the octamer by insertion of one and two two-coordinated molecules, respectively, into the D_{2d} cube edges. The two heptamer isomers are obtained by removal of a single water molecule from the S_4 octamer cube. The $n = 8-10$ clusters correspond to relatively regular structures, characterized by two distinct groups of O··O bond lengths and corresponding stretch frequencies. The more strained and asymmetric heptamers include a broad range of hydrogen bonded configurations, which are reflected by a complex OH stretch spectrum with numerous peaks. Two additional low energy decamer structures were investigated, which correspond to two fused pentamer rings. Following past suggestions, we further explored the possibility of parameterizing OH bond frequency as a function of the electric field at the H atom.

I. Introduction

The study of weakly bound clusters of molecules opens new, exciting possibilities for exploring the structural transition from the molecular constituents to the condensed phases. Of particular interest are water clusters, since they serve as excellent model systems for testing our understanding of hydrogen bonding in water and for calibrating potentials. Since the original matrix isolation studies of the water dimer by Pimentel,[1] experimental methods to determine structure, spectra, and other properties of the water clusters have progressed dramatically; in parallel, a large number of theoretical studies has been carried out. It is noted that the pertinent literature on H_2O clusters is very extensive and would comprise a citation list of unreasonable length; therefore, our list includes only a representative set, most directly relevant to the present study.

For the water dimer, a sequence of experimental and theoretical studies (see, e.g., refs 2 and 3) demonstrated conclusively a near-linear hydrogen-bonded global minimum on the potential energy surface (PES). Dimer data include a wealth of information on the water PES at the level of a pair interaction, as indicated by recent accurate calculations of rovibrational energy levels.[4] However, it is known that many-body interactions affect significantly water properties in condensed phases, and provide a significant fraction of the binding energy. Water clusters larger than dimers are an excellent source of information on such interactions.

$(H_2O)_n$, $n \geq 3$ clusters have been investigated extensively for a long time, in theoretical studies employing electronic structure techniques (e.g., refs 5−23), a variety of analytical potentials (e.g., refs 24−32), and a combination of both (e.g., refs 33−41). For $n = 3-5$, a cyclic lowest energy structure has been predicted, with the basic structural unit of a single proton donor−single acceptor (DA) water molecule. A transition toward three-dimensional structures was obtained near $n = 6$ (e.g., 11, 15, 33, 34, 40). For the octamer, two very stable cubic structures (S_4 and D_{2d}) have been predicted.[28,33,36] There has been a discussion in the literature concerning the possible participation of such cubic units in larger clusters versus evolution toward structures with larger water rings.[19,27−29,32,37,38] The difficulties associated with the modeling of structures and spectra of clusters increase significantly as a function of size. There is a dramatic increase in the number of adjacent low lying minima. Calculations of energy ordering of the different isomers are complicated by inaccuracies in both empirical and ab initio potentials and by possibly large zero-point energy (ZPE) effects. Accurate calculations of vibrational energy levels are becoming increasingly difficult.

The main experimental difficulty in the study of $(H_2O)_n$, $n \geq 3$ has been the measurement of spectra of *size selected* neutral clusters. This barrier has been surmounted recently in a number of laboratories. A series of far-infrared vibration-rotation-tunneling[42] and infrared[43,44] laser spectroscopic studies dem-

10.1021/jp990546b CCC: $18.00
Published on Web 06/09/1999

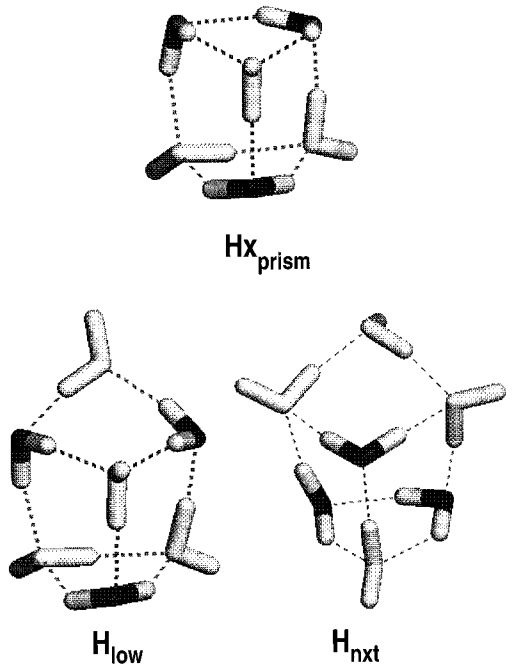

Figure 1. Structures of hexamer-prism and two heptamers after MP2 minimization. The O atoms of DDA molecules are marked black.

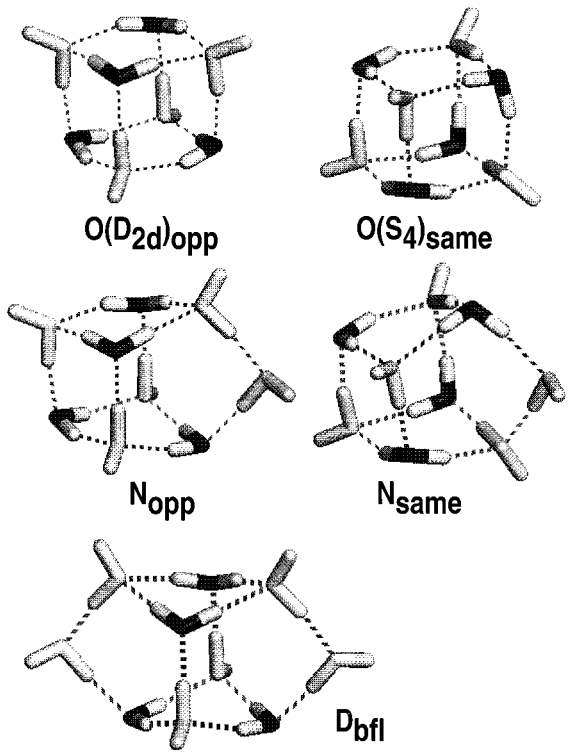

Figure 2. Structures of $n = 8-10$ clusters after MP2 minimization. The O atoms of DDA molecules are marked black. Top: octamers; middle: nonamers; bottom: D_{bfl} decamer structure. The structures are shown from the point of view emphasizing the evolution from octamer cubes.

onstrated conclusively a cyclic structure for $n = 3-5$ and a transition toward a three-dimensional cage structure at $n = 6$.[45,46] Similar conclusions were drawn from the double resonance ion-dip infrared experiments on water clusters connected to benzene[15,47] and phenol.[48,49] The two stable symmetric cube structures of the octamer were first reported for the $(H_2O)_8$-benzene cluster.[50] For pure water clusters, the two cubes were demonstrated in our recent study of size selected $(H_2O)_n$ spectroscopy.[51] The cube structures were also shown to be present in water clusters with a phenol chromophore.[52]

The present study belongs to a series of our investigations of $(H_2O)_n$ structures and spectra in the three-dimensional size regime $n = 7-10$. Size selected OH spectra of the pertinent clusters have been recently measured and interpreted with the help of calculations.[51,53] The structures, which are the focus of the present study, are shown in Figures 1−3. Six of these structures (H_{low}, H_{nxt}, $O(D_{2d})_{opp}$, $O(S_4)_{same}$, N_{opp}, and D_{bfl}) were used to assign the experimental spectra. In addition, the set includes two decamer structures (D_{same} and D_{opp}), which seem to correspond to the lowest decamer potential minima; these minima are, however, destabilized by ZPE effects.[51] Limited calculations are also presented for the hexamer prism, mainly for comparison with other studies. The structures shown in Figures 1−3 can be considered loosely as members of a series, derived from the two lowest energy octamer cubes by either insertion or removal of water molecules. The main structural units in these clusters are three-coordinated molecules of two varieties: double donor−single acceptor (DDA) and single donor−double acceptor (DAA). As discussed below, H atoms of DDA molecules form relatively weak hydrogen bonds, while H atoms of DAA form relatively strong ones.[15,47,51,54]

Extensive use of OH stretch spectroscopy as a structural probe of clusters and other water-containing systems is related to the great sensitivity of the OH stretch frequency to hydrogen bonding. A strong hydrogen bond results in frequency red-shift of hundreds of inverse centimeters. Moreover, the spectra are sensitive to hydrogen bond geometry and coordination.[7,47,51,54] One of the chief aims of our studies is to put the connection between the hydrogen bond strength and geometry and the OH spectra on a more quantitative basis.

MP2 level ab initio calculations are presented of minimum energy structures and of harmonic frequencies for all of the above mentioned $n = 6-10$ cluster structures. To the best of our knowledge, ab initio results at a correlated level are reported here for the first time for $n = 9$, 10 (inclusion of correlation is necessary for calculations of OH stretch spectra[15,55]). Calculations on the present level are sufficient to reproduce qualitatively the observed range of spectral lines, and the approximate frequency shift characteristics of different hydrogen-bonded coordinations. However, quantitative reproduction of OH stretch spectra requires correlated ab initio calculations on a level which is much too high for systems of that size.[55] We then attempted to construct an empirical model capable of a better representation of the experiment.

An ultimate tool for interpreting the connection between structure and spectroscopy of H_2O containing systems would be an accurate *flexible* water potential. Parameterization of flexible water potentials is much less advanced than parameterization of the rigid ones. A usual way for constructing a flexible potential is to combine a reasonable rigid PES with a sum of intramolecular terms parameterized for gaseous H_2O (see, e.g., refs 25, 56). However, intramolecular properties change as a result of hydrogen bonding, e.g., bond dipole derivatives increase dramatically and change direction,[57] and the bond coupling constant changes sign[58,59] (see also discussion below).

Here, a different approach was adopted for constructing an empirical model of the OH stretch spectra. The main challenge was to establish the relation between the bond frequency and the strength and the geometry of hydrogen bonding. Combination of quantitative data from cluster spectroscopy with qualita-

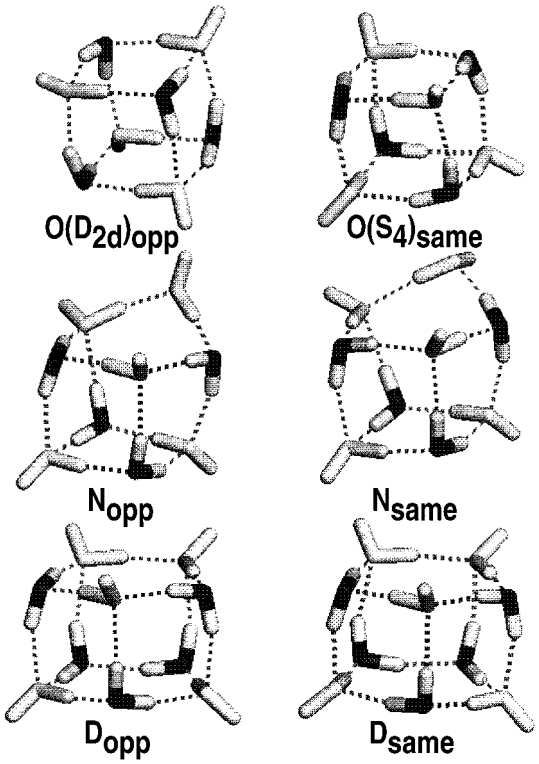

Figure 3. Structures of $n = 8-10$ clusters after MP2 minimization. The O atoms of DDA molecules are marked black. Top: octamers; middle: nonamers; bottom: decamers. The $n = 8-9$ structures are the same as in Figure 2, shown from a different point of view. All of these structures can be considered as two fused rings; the OH··OH·· OH·· pattern in the top ring is oriented either in the opposite direction (left structures) or the same direction (right) as the bottom ring.

tive ideas from ab initio studies seems a viable basis for calibrating such a model. In ab initio studies of ref 60, it was suggested that the OH stretch frequency should be a parabolic function of $E_{||}$, the electric field component parallel to OH, at the H atom. Physically, a hydrogen bond can be viewed as a strong electrostatic interaction, so $E_{||}$ is a reasonable measure of the bond strength. The idea was shown to work qualitatively for the H_2O point charge system and for $Mg^{2+}\cdot(H_2O)_n$ clusters.[60]

In the present model, this idea was generalized by assuming that the OH stretch frequency in water clusters is *some* (not necessarily parabolic) function of $E_{||}$, where $E_{||}$ is calculated as the field of the fixed charges and the induced dipoles of a polarizable potential denoted EMP.[61] In our initial study of $(H_2O)_n$, $n = 8-10$, (ref 51) the calibration of the $\omega(E_{||})$ function was performed using minimum energy conformations of the cyclic water clusters ($n = 3-5$) and of the octamer cube. The nonamer and decamer structures were suggested on the basis of comparison to experiment of calculated spectra employing this parameterization. However, the much more complex heptamer spectra were not reproduced. Moreover, a parameterization based on properties of the minimum does not take into account intermolecular delocalization. In fact, the ground state of the small cyclic clusters was shown to be above transition barriers between several minima.[35,42] Even the more rigid $n = 6-10$ clusters cover a considerable range of zero-point motion (ZPM). It has been shown in a number of studies,[78,79] that intermolecular delocalization around the minimum may affect substantially intramolecular cluster spectra. This is because a minimum is a special location of particularly strong hydrogen bonds, and ZPM brings the cluster away from the minimum. A new parameterization and a treatment of OH stretch spectra including ZPM effects was introduced in a recent letter on the heptamer,[53] and is described in more detail in this article.

Ab initio methods and results are described in section II. Section III describes results obtained with the EMP potential, including cluster spectra, dipoles, and energetics. Energies and spectra obtained in EMP and ab initio calculations are compared to each other and to experimental data. In section IV, the relation between clusters and condensed H_2O phases is discussed briefly. Results are summarized in section V. The measurements of the pertinent OH stretch spectra of size selected clusters are summarized in the Appendix; the experiments were reported in refs 51 and 53.

II. Ab Initio Calculations

A. Cluster Structures. Since an exhaustive search for the global minimum energy conformation is not practicable at the ab initio level for water clusters in the size range $n = 7-10$, the information based on an analytic water potential is a useful guide to the low energy topologies. The input configurations to ab initio minimizations are low energy minima obtained previously[51,53] with the EMP potential,[61,62] which is described in section III. The search for the lowest energy structures was carried out by thousands of minimizations employing random initial conditions. The initial conditions corresponded to two water rings randomly displaced and rotated with respect to each other; in addition, "noise" was added to the center-of-mass water coordinates.

The structures selected for investigation in the present study are shown in Figures 1−3, together with the nomenclature used throughout the article. The figures display the structures after MP2 minimizations; the input structures from EMP minimizations are visually similar. In each of the structures there is an equal number of DDA and DAA molecules; the heptamers, the nonamers, and one of the decamers include in addition two-coordinated DA molecules. The O atoms of the DDA molecules are marked black in the figures. The O atoms of DAA and DA are marked white (the two types of molecules can be easily distinguished by inspection). The structures shown in Figures 1−3 can be considered loosely as members of a series, derived from the two low energy octamer cubes by either insertion or removal of water molecules. The two "parent" octamer units, denoted $O(D_{2d})_{opp}$ and $O(S_4)_{same}$, are shown at the top of Figures 2 and 3; the experimental spectra were assigned to a mixture of both isomers. Figure 2 shows also two nonamer structures N_{opp} and N_{same} and a decamer structure D_{bfl} ("butterfly"); the latter structures are shown from the point of view which emphasizes the structural evolution from the octamer cubes. The nonamer and the decamer structures are derived from the octamers by insertion of one and two two-coordinated DA molecules, respectively, into the cube edges. The N_{opp} and D_{bfl} minima were selected for this study, since their calculated OH stretch spectra were found to match best the experiment.[51] N_{opp} is the lowest nonamer minimum found, N_{same} is the next one. D_{bfl} is *not* the lowest decamer minimum. The lowest minima, D_{same} and D_{opp}, which are shown at the bottom of Figure 3, can be viewed as two fused pentamer rings. The D_{same} and D_{opp} minima can be derived from the octamer cubes, by multiplying one of the two-molecule edges connecting the oriented rings; note the repetition of the vertical edges in the back "wall" of the two decamers, as shown in Figure 3. The D_{same} and D_{opp} structures are destabilized by ZPE effects and, after inclusion of ZPE, become nearly isoenergetic with D_{bfl}. Comparison with experiment suggests that, in reality, D_{bfl} is lower in energy; however, the currently available methods appear to be insufficiently accurate for calculation of small energy differences.

TABLE 1: Calculated Properties of the Water Monomer in DZ1P Basis Set on HF and MP2 Levels[a]

	SCF		MP2		
parameter	ν	I	ν	I	exptl
ν_1	4113	22.8	3922	11.4	3832
ν_2	1711	122.0	1617	104.9	1649
ν_3	4265	64.1	4060	39.0	3943
$\Delta\nu_{13}$	152		138		110

	SCF		MP2		
parameter	ν	I	ν	I	exptl
R(OH) (Å)	0.9543		0.9699		
HOH	106.7°		104.9°		
$\mu(D)$			2.192		1.855
α (a.u.)			5.113		9.94
E_{tot} (hartree)	−76.0375667		−76.2202658		
ZPE (kcal/mol)	14.423		13.721		

[a] Harmonic frequencies ν_i in cm^{-1}; intensity I in KM/mol. Experimental data are from a compilation of ref 55.

All of the structures with the subscripts "opp" and "same" can be viewed as two fused *oriented* rings. This point of view is demonstrated in Figure 3. In all of the structures, the closed ring pattern OH··OH···OH·· in the bottom ring is oriented in either the same or the opposite direction as in the top ring. The two lowest "same" and "opp" isomers of each cluster are close in energy.

The two heptamer structures H_{low}, and H_{nxt}, shown in Figure 1, can be derived from the $O(S_4)_{same}$ octamer cube by removal of either one DDA or one DAA water molecule. Alternatively, they can be obtained by insertion of one two-coordinated water molecule to either top or bottom triangular base of the hexamer prism. The H_{low} and H_{nxt} minima are the lowest energy structures found for $n = 7$, in accord with past theoretical predictions.[33] The experimental spectra include contributions from both heptamer isomers.[53]

Finally, limited calculations are presented for the hexamer prism Hx_{prism}, chiefly for the purpose of comparison with other studies. The prism, shown in Figure 1, top, can be considered the lowest member of the series, obtained by removal of the DA molecule from either of the heptamers. Extensive past studies of $n = 6$ (e.g., refs 11, 15, 16, 38, 34, 40, 45) suggest, that the prism is one of the lowest hexamer minima, and perhaps the lowest one, which is however destabilized with respect to the experimentally observed "cage" structure by ZPE effects.[45]

Note that all ofthe structures in Figures 1−3 (except $O(D_{2d})_{opp}$) have isoenergetic isomers which can be obtained by reflection. For example, exchange of the left and the right hand side in all structures shown in Figure 1 results in obviously isoenergetic structures, which cannot be overlapped with the original ones.

B. Methods of Ab Initio Calculations. The EMP minima were used as input for ab initio optimizations at two levels:

TABLE 2: Cluster Energies[a]

	7		8		9	
n	H_{low}	H_{nzt}	D_{2d}	S_4	N_{opp}	N_{same}
SCF:E_{tot}	−532.357117	−532.351509	−608.410852	−608.411231	−684.463579	−684.463018
SCF:ZPE	118.053	118.141	136.23	136.299	153.055	153.094
SCF:D_e	−46.894	−46.496	−58.894	−58.717	−67.361	−66.601
SCF:D_0	−29.802	−29.316	−38.048	−37.802	−44.113	−43.355
SCF:$D_{e,rel}$	−46.099	−45.636	−57.949	−57.766	−66.253	−65.579
SCF:$D_{0,rel}$	−29.007	−28.456	−37.103	−36.851	−43.005	−42.333
MP2:E_{tot}	−533.679125	−533.679111	−609.933349	−609.934137	−686.176985	−686.176587
MP2:ZPE	114.883	115.040	132.42	132.511	149.020	149.002
MP2:D_e	−55.244	−54.775	−70.255	−70.017	−80.197	−79.585
MP2:D_0	−36.407	−35.775	−47.603	−47.274	−54.666	−54.072
MP2:$D_{e,rel}$	−52.041	−51.529	−66.091	−65.849	−75.289	−74.581
MP2:$D_{0,rel}$	−33.230	−32.530	−43.438	−43.106	−49.795	−49.068
EMP(r):D_e	−57.014	−56.915	−71.267	−71.322	−80.541	−80.236
EMP(r):D_0	−38.8	−38.5	−48.4	−48.5	−55.2	−54.8
EMP(fl):D_e	−58.886	−58.873	−73.714	−73.789	−83.189	−82.927
EMP(fl):D_0	−44.5	−44.4	−55.9	−56.1	−64.2	−63.7

	10		
n	D_{opp}	D_{same}	D_{bfl} (trans)
SCF:E_{tot}	−760.518576	−760.518921	−760.516006
SCF:ZPE	170.670	170.742	169.821
SCF:D_e	−76.445	−76.201	−75.5275
SCF:D_0	−50.004	−49.689	−49.936
SCF:$D_{e,rel}$	−75.161	−74.904	−74.259
SCF:$D_{0,rel}$	−48.721	−48.391	−48.668
MP2:E_{tot}	−762.424686	−762.425409	−762.420022
MP2:ZPE	166.086	166.181	165.495
MP2:D_e	−91.452	−91.127	−89.764
MP2:D_0	−62.532	−62.156	−61.479
MP2:$D_{e,rel}$	−85.631	−85.291	−84.263
MP2:$D_{0,rel}$	−56.755	−56.319	−55.978
EMP(r):D_e	−91.934	−92.013	−89.667
EMP(r):D_0	−62.8	−62.6	−62.0
EMP(fl):D_e	−94.956	−95.060	−92.503
EMP(f):D_0	−72.8	−72.9	−72.1

[a] E_{tot} is in hartree, the remaining values are in kcal/mol. D_e and D_0 corrected for deformation energy are given as $D_{e,rel}$ and $D_{0,rel}$; see section IIB. EMP(r) and EMP(fl) denote a rigid and a flexible version of the empirical potential.

(a) the low-cost SCF and (b) MP2 employing the double-zeta Dunning basis (9s5p1d)/[3s2p1d] for the oxygen atom and (4s1p)/[2s1p] for the hydrogen atom, plus polarization functions with exponents 0.9 for O and 1.0 for H (DZ1P basis)[63]). This basis set is not ideal for water clusters, but it is the largest that could be realistically used with our computer resources for $n = 10$ geometry optimization at a correlated level. This basis was retained for smaller clusters as well, to obtain trends as a function of size on a consistent level of accuracy. We expect the MP2 minimum geometries to be fairly accurate; however, the interaction energies may be affected by the errors in the description of the monomer electric properties, as shown in Table 1, and other limitations of the supermolecular method.[55]

It was suggested in many papers that electron correlation is necessary to describe the structure and energetics of hydrogen-bonded clusters. Treatment of the correlation problem at the second-order perturbation theory (MP2) level was found to produce more accurate results for the structure, vibrational frequencies, and dipole moment as compared to SCF results.[17] A related study[64] commented that correlated calculations are crucial for the two-body contributions to the energy. Ab initio studies of frequency shifts in water with respect to monomers demonstrated an underestimation of shifts by a factor of 1/2−2/3 on the SCF level.[55,65] On the other hand, it was shown that for some fairly small basis sets (e.g., 4-31G) one can reproduce qualitatively frequency shifts for water clusters, already on the SCF level, due to error cancellation.[7] Still, it appears safer to use a better basis on a correlated level.

The use of the DZ1P basis introduces a sizable basis set superposition error (BSSE). We have used the counterpoise correction method (CP) to account for BSSE in the calculations of the binding energy D_e at the minimum.[66] We are aware of the fact that this approach is far from perfect: BSSE should be considered in each optimization step, not only for the optimized final structures; however, the appropriate minimization code is not yet available. The use of CP correction by Boys and Bernardi,[66] and the problems associated with it, are discussed, e.g., in refs 67−69. Some authors note the overestimation of the effect in this method correction.[11,67,68] Still, we prefer to apply the CP correction on account of the limited size of the basis.

Inclusion of deformation correction is a relatively new issue. At cluster equilibrium, the monomer is deformed slightly with respect to the isolated monomer equilibrium geometry. To account for that, a modification of the Boys−Bernardi procedure has been proposed recently.[70,71] E_{def} denotes the energy required to deform the monomers (calculated in the monomer basis set) from their optimal geometries when isolated, to their optimal geometries when interacting with each other in the complex. The binding energy D_e is calculated as the energy of the cluster at the minimum, minus the energy of isolated monomers at the same geometry, plus E_{def}. The latter correction is non-negligible and amounts to 6−7% of $|D_e|$ (i.e., several kcal/mol) in MP2; see Table 2.

The ab initio calculations were carried out with a suite of Gaussian 94[72] programs. Full geometry optimizations were carried out using the most stringent internal criteria of Gaussian 94 (VERYTIGHT option)[72] at the SCF and MP2 (frozen core approximation) levels. Harmonic SCF and MP2 frequencies and infrared intensities were calculated using analytic second derivatives (except for $n = 10$, where the numerical option was used). The calculated energies are shown in Table 2. D_e denotes BSSE corrected minimum energy. The dissociation energy D_0 was obtained by adding to D_e zero-point energy correction Δ(ZPE) calculated with the unscaled harmonic frequencies (Δ(ZPE) is the difference between the sum of monomer ZPE, and the cluster ZPE). D_e and D_0 corrected for deformation are also given in the table, as $D_{e,rel}$ and $D_{0,rel}$. Figures 4 and 5 show, respectively, the distributions of hydrogen-bonded O··O distances and the calculated spectra, obtained with MP2. Listing of unscaled ab initio frequencies and intensities can be found in Tables 1−9 of the supplementary material. In Figure 5, for the sake of comparison with experiment, the harmonic ab initio MP2 frequencies were rescaled uniformly by the ratio of the experimental and the calculated dangling OH frequencies (0.943). The experimental cluster spectra can be seen in Figure 6 (together with some condensed phase spectra, which are shown for comparison[73,74]).

Monomer geometry, unscaled frequencies, and electrical properties are presented in Table 1. At the HF level, the frequencies are all overestimated in the DZ1P basis set. The electron correlation red-shifts the frequencies. At the MP2 level, the OH stretching frequencies are still overestimated by some 100 cm^{-1}, while the bending frequency is underestimated by 32 cm^{-1}. Let $\Delta\nu_{13}$ be the harmonic vibrational frequency difference between the asymmetric and symmetric OH stretching modes. Experimentally, $\Delta\nu_{13}$ is 110 cm^{-1}, while the MP2 value is 138 cm^{-1}. The error in the bond coupling constant is more serious than it looks, since potential coupling contributes only about half of $\Delta\nu_{13}$ (the other half is contributed by the momentum coupling). This is an inherent inaccuracy in the MP2 prediction of harmonic water frequencies, even in a very large basis set.[55]

The calculations for the hexamer prism Hx_{prism} are reported here to test the validity of the present computation against results obtained by other authors in larger basis sets. The BSSE-corrected binding energy calculated by us in MP2/DZ1P is −43.602 kcal/mol; after correction for the relaxation energy of the monomers, the binding energy $D_{e,rel}$ is equal to −41.075 kcal/mol. The BSSE-corrected binding energy D_e of Hx_{prism} in the MP2/aug-ccpVDZ* basis is −40.22 kcal/mol.[14] The BSSE-corrected D_e obtained in ref 11 in their largest basis set (MP2-(FC)(HZ4P(1fg,2d)++) is −43.64 kcal/mol (the uncorrected value is −46.61 kcal/mol). In the DZ1P basis set, the calculated OH frequency shifts in the hexamer, relative to the mean frequency of the two OH monomer modes (3991 cm^{-1}) are as follows: −764, −461, −377, −347, −219, −194, −169, −130, −113, −43, −35, −26 cm^{-1}. These values can be compared to the ones calculated in the 6-31+G(D2d,p) basis set in ref 15 (here the reference frequency was 3900 cm^{-1}): −685, −439, −362, −314, −212, −191, −116, −100, −73, +2, +6, +8 cm^{-1}. The qualitative agreement seems not unreasonable. Finally, one may compare the (unscaled) calculated frequency range spanned by the OH stretch spectra of the two heptamers (415 cm^{-1} in SCF and 850 cm^{-1} in MP2, see Table 1 of the supplementary material, and Figure 5), with the experimental range which is close to 800 cm^{-1} (see Figure 6). The underestimation of the frequency shifts on the SCF level is in accord with previous experience,[55,65] while the qualitative agreement with experiment on the MP2 level is encouraging.

Let us conclude this paragraph: The accuracy of the presently accessible ab initio methods (and of empirical potentials as well) is insufficient for a quantitative calculation of cluster properties in the size range considered. One can however hope for qualitatively reasonable structures and spectra, useful for the interpretation of the experimental data.

C. Cluster Structures and Spectra from Ab Initio. *General Structural Features.* Figure 4 shows a distribution of O··O

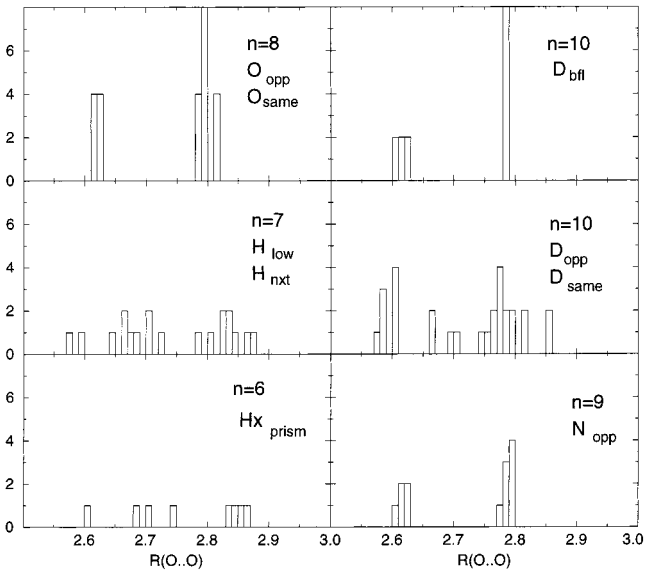

Figure 4. The histogram of near neighbor R(O···O) distances between pairs of hydrogen-bonded molecules in water clusters (MP2).

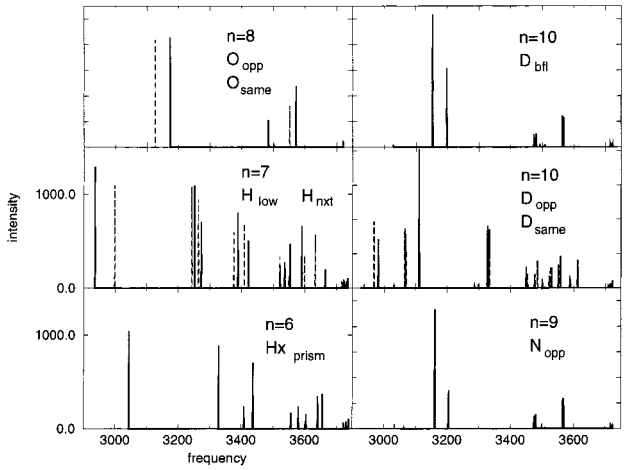

Figure 5. Calculated spectra for water clusters from $n = 6$ to $n = 10$ obtained by MP2 normal mode analysis. Normal frequencies were rescaled by 0.943. Intensity units: thousands of Km/mol. Note the difference in intensity scales for the different sizes; the spacing between the tick marks on the *y*-axis is 1000 Km/mol for all graphs. In $n = 7$, 8, 10 spectra, the peaks due to the second isomer (H_{nxt}, $O(S_4)_{same}$, and D_{same}) are dashed.

distances between hydrogen-bonded pairs of molecules. As already noted in the past, the O··O distances in hydrogen bonds emanating from DDA (i.e., in which DDA acts as a proton donor) tend to be longer than bonds emanating from DAA, and the corresponding OH bond frequencies tend to be higher (e.g., refs 7, 15, 47, 51, 54). Henceforth, the two kinds of hydrogen bonds are denoted as DDA and DAA bonds. We suggest the following physical reason for this difference between DDA and DAA bonds: The bonding via the H atom tends to be directional, i.e., the energy (and the frequency) is lowered if the O atom of the bonding partner lies near the OH bond axis. On the other hand, the bonding via O is less directional, i.e., the OH bond of the partner can point toward O from a broad range of directions at a small energy expense, as long as the OH··O angle is reasonably close to 180°.[75,76] Therefore, the DAA molecules manage to optimize the hydrogen bond geometry of the single bonded H atom much better than the DDA molecules, which have to accommodate simultaneously two H atoms within the constraints of the hydrogen bond network; one should note that the O···O···O angles between hydrogen bonds made by a DDA molecule in cage clusters are substantially smaller than the HOH angle in water. The result is the observed difference between the DDA and DAA in near neighbor O··O distances and in OH frequencies.

On the basis of O··O distance distribution (Figure 4), the cluster structures studied here can be loosely divided to "crystal-like" and "amorphous". A crystal is characterized by a discrete distribution of interatomic distances; while in a topologically disordered amorphous solid the distribution is continuous. The clusters include two physically distinct categories of bonds (DDA and DAA bonds). In the crystal-like clusters ($O(S_4)_{same}$, $O(D_{2d})_{opp}$, N_{opp}, D_{bfl}), all bonds of the same category have approximately the same lengths; the O··O distance distribution is therefore doubly peaked, with a gap in between. In the remaining amorphous clusters, DDA bonds still tend to be longer than DAA; however, a broad length distribution is obtained, without a pronounced gap separating the two categories.

Crystalline Clusters $O(S_4)_{same}$, $O(D_{2d})_{opp}$, N_{opp} D_{bfl}. As noted above, in these structures one obtains two *well separated and distinct* groups of nearest neighbor O··O bond lengths, near 2.62 and 2.79 Å, corresponding to DDA and DAA hydrogen bonds, respectively (see Figure 4). The narrowness of the two R(O·· O) distributions seems to be due the fact that all bonds between three-coordinated molecules are of the same asymmetric type, i.e., DDA molecules are connected only to DAA molecules and vice versa. Even the DA molecules in N_{opp} and D_{bfl} adapt themselves to the crystalline tendency of the rest and adopt O··O distances of 2.62 Å, which are close to DAA.

As a result, the calculated OH stretch spectrum of crystalline clusters contains two well separated DAA and DDA bands (see Figure 5). In addition, a third band is obtained for the dangling OH (dang-OH) bonds at the cluster surface. These results are in qualitative agreement with experiment (Figure 6). The rescaled DDA/DAA frequencies correspond to mean frequencies near 3520/3150 cm^{-1}, in reasonable agreement with the experimental values near 3550/3070 cm^{-1}. The very large differences in intensities between the DAA, DDA, and dang-OH bands (see Figure 5) are in disagreement with experiment. (Note however that the experimental spectra pertain to dissociation probabilities, and the infrared absorption intensity is only one of the factors that determine the signal;[51] see Appendix on experimental details.)

Another feature which was not reproduced by the MP2 calculations is the splitting between the DDA symmetric and asymmetric stretch $\Delta\nu_{13}$, which is 90 cm^{-1} in the calculation, and 24−30 cm^{-1} in the experiment. Note that in the $n = 8-10$ clusters, the measured $\Delta\nu_{13}$ value is reduced by more than a factor of 3 with respect to the gas phase! On the other hand, a similarly small splitting of 45 cm^{-1} was measured for H_2O molecules isolated in the D_2O ice.[77] The value of $\Delta\nu_{13}$ is dominated by a combined effect of intramolecular momentum coupling between two OH bonds sharing an O atom and a potential coupling term of the form $k\delta r_1\delta r_2$ between the two bonds. In the gas phase, the two terms reinforce each other, resulting in $\Delta\nu_{13} = 110$ cm^{-1}. The splitting that would be obtained with momentum coupling only, while setting k to zero, is about 60 cm^{-1}. To reproduce the difference between gaseous H_2O and ice, one must change both the sign and the size of k with respect to the gaseous value to obtain partial cancellation of momentum and potential coupling[54,58] (see section III-2 below). While the calculated change in $\Delta\nu_{13}$ is in the right direction (see also ref 7), it is much too small. Calculation of quantities such as bond coupling constants or intensities requires

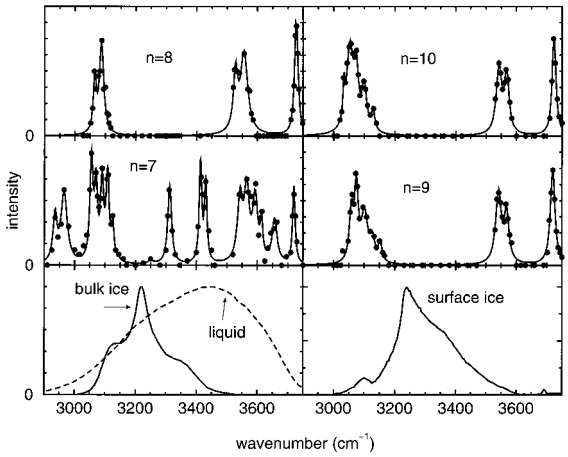

Figure 6. Four top panels: experimental OH stretch spectra for clusters, measured as the dissociated fractions. Left, bottom: infrared absorption spectrum of an ice film at 90 K[73] and of liquid water at 313 K.[74] Right, bottom: spectrum of an ice nanocrystal surface at 120 K, obtained as described in ref 73.

a very high-level correlated calculation, as shown already for the monomer.[55] This result underscores the need for experimental input (in addition to ab initio calculations) for calibrating a good flexible potential for water.

One may note, finally, that the second nonamer structure N_{same} is characterized by an intermediate behavior between the crystalline clusters, and the "amorphous" ones described below. The distribution of DDA and DAA bond lengths is broader than in N_{opp}. The two hydrogen bonds near the DA molecule adopt intermediate bond lengths (2.72 and 2.73 A). A collective oscillation of these bonds results in a spectral feature just below 3400 cm^{-1}, within the spectral gap of the crystalline clusters.

"Amorphous" Clusters Hx_{prism}, H_{low}, H_{nxt}, D_{opp}, D_{same}. These clusters are characterized by much broader distributions of DDA and DAA bond distances (Figure 4) which are not well separated. The structures include odd membered rings with symmetric bonding configurations DDA−DDA and DAA−DAA, which are absent in the crystal-like cluster family. The O··O distances in DAA−DAA pairs are significantly longer than DAA bonds in asymmetric pairs, presumably because of repulsion between adjacent dangling bonds. The O··O distances in DDA−DDA pairs are, for some reason, shorter than DDA bonds in asymmetric pairs. These new bond lengths appear in the gap between the two peaks in the R(O··O) distribution of crystal-like clusters. In $n = 7$, the R(O··O) distances in the vicinity of the DA molecules appear in the gap as well. Additional contributions to broadening are due to the presence of strained three-membered rings (in Hx_{prism} and in the two heptamers) and to the asymmetry of the heptamer and the decamer structures. As a result, one finds both some very short (asymmetrically connected) DAA bonds, and some very long (asymmetrically connected) DDA bonds.

In amorphous structures, one finds near neighbor R(O··O) ranging from 2.58 to 2.89 Å, instead of two sharp peaks near 2.62 and 2.79 Å, as in the crystalline case. The calculated amorphous spectra, which largely mimic the R(O··O) distributions, contain numerous peaks, rather than two well-defined DDA and DAA features (see Figure 5). This result is in qualitative accord with the experimental heptamer spectrum, which includes *six* hydrogen-bonded bands, rather than two, as in the case of crystalline clusters $n = 8-10$ (see Figure 6). Although the MP2 calculation did not reproduce quantitatively the complex experimental spectral pattern for $n = 7$, it did

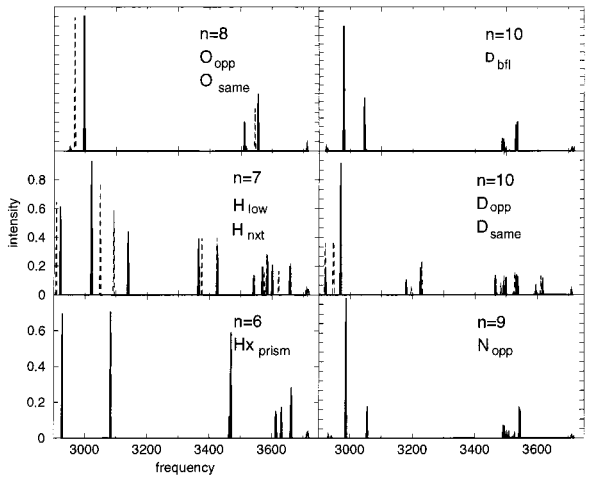

Figure 7. Calculated spectra for water clusters from $n = 6$ to $n = 10$ using EMP potential, without ZPM averaging. That is, bond frequencies are calculated using $E_{||}$ at the EMP(fl) minimum. In $n = 7$, 8, 10 spectra, the peaks due to the second isomer (H_{nxt}, $O(S_4)_{same}$, and D_{same}) are dashed. The intensities are in the same relative units for all clusters. Note the difference in intensity scales for the different sizes; the spacing between the tick marks on the *y*-axis is 0.2 units for all graphs.

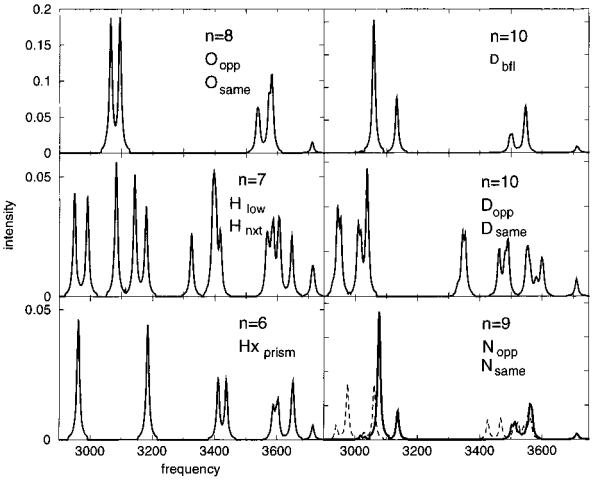

Figure 8. Calculated spectra for water clusters from $n = 6$ to $n = 10$ using EMP potential, with ZPM averaging. To facilitate comparison with experiment, the lines were assigned Lorentzian shapes of width 10 cm^{-1}. For the nonamers, two isomer spectra were drawn separately, the dashed line corresponds to N_{same}. The intensities are in the same relative units for all clusters. Note the difference in intensity scales for the different sizes; the spacing between the tick marks on the *y*-axis is 0.05 units for all graphs.

reproduce the presence of two very low frequency peaks, below 3000 cm^{-1}. Each heptamer contributes one peak which corresponds to a particularly short vertical DAA bond connecting a trimer to a tetramer; the shortest bond of the "parent" Hx_{prism} structure is also present in the equivalent location (see the rightmost vertical DAA bond in all three structures in Figure 1).

III. Calculations of Cluster Spectra and Energetics with the Empirical Potential

The calculations with EMP were carried out to supplement the information on cluster energetics and dipoles. However, the main focus was on the spectra. We attempted to construct an empirical model capable of reproducing the experiment. As described in the introduction, the model is based on the parametrization of the OH bond frequency as a function of the electric field at the H atom, while including intermolecular ZPM

effects. The spectra calculated without and with ZPM effects are shown in Figures 7 and 8.

A. Technical Details *1. The EMP Potential.* The empirical potential that is used here is a modified version of an empirical polarizable water potential proposed in ref 62. The monomer electric properties are represented by three point charges (two positive ones on the H atoms, and a negative one on the water bisector) and a single dipole polarizability center. At short distances, the point charge/point polarizability description may break down, resulting in artificially large induced dipoles. To remedy this artifact, distance-dependent shielding was introduced of the electric field induced by the charges at the point polarizability site. The repulsive core of the potential was represented by exponential interatomic terms. The modification of the potential was carried out by us,[61] in an effort to provide a balanced description of all water phases (solid, liquid, and clusters), and in particular to make the observed ordered ferroelectric form of ice energetically favorable with respect to proton-disordered ice.[80] The parameters modified with respect to the original version are $r_s = 1.25$ Å and $b_{oo} = 2.65$ au;[61] moreover, the polarizability center was shifted by 0.48 Å from the original location at the O atom (down the bisector of H_2O and toward the middle of the molecule; the latter shift stabilizes the ferroelectric $Cmc2_1$ form of ice with respect to disordered ice). The EMP potential is rigid. Some calculations were carried out with a simple flexible extension of EMP,[61] in which the following intramolecular term was added to the potential $V_{\text{intra}} = \sum_{m=oh1,\ oh2,\ hh} 0.5k_m(r_m - r_m^0)^2 + k'(r_{hh} - r_{hh}^0)(r_{oh1} + r_{oh2} - r_{oh1}^0 - r_{oh2}^0)$, with r_m^0 adopted from the monomer geometry of the corresponding rigid PES ($r_{oh} = 0.9572$ Å, $r_{hh} = 1.5139$ Å). The force constants are $k_{oh} = 0.5924$ au, $k_{hh} = 0.1317$ au, and $k' = -0.12$ au. This flexible extension does *not* represent a serious effort to represent the dependence on intramolecular coordinates; it is used here for rough estimates of flexibility effects, e.g., on cluster energetics. The flexible extension is denoted below EMP(fl). In passages in which both the rigid and the flexible versions of EMP are discussed, EMP(r) denotes the rigid version. Otherwise, EMP denotes the rigid version.

One may note that the qualitative geometric properties of cluster minima calculated with EMP are in accord with ab initio, except that DAA and DDA bond lengths are longer. In crystalline clusters, DAA and DDA O··O distances obtained with EMP(fl) are at 2.75 and 2.85 Å, respectively, rather than 2.62 and 2.79 Å, as in MP2.

2. A Scheme to Calculate OH Spectra. As in our previous studies of ice[54,59] and clusters,[51,53,79] OH bonds are treated as local Morse oscillators. The ground state is approximated as a product of ground Morse states for all of the OH bonds, and the ground state energy as a sum of Morse ground state energies. An excited state is expanded in the exciton basis $\sum c_i|1_i\rangle$, where $|1_i\rangle$ is a product basis state with one quantum in bond i and zero quanta in the remaining bonds. The crucial ingredient in constructing the Hamiltonian matrix is the dependence of the bond Morse parameters on the strength of the hydrogen bonds; this issue is discussed separately, in the next subsection.

The OH bonds are coupled via intra and intermolecular coupling. The intramolecular coupling is a sum of momentum coupling $p_1p_2\cos(\text{HOH})/m_o$ between two OH bonds sharing an O atom,[81] and a potential coupling term of the form $k_{\text{intra}}\delta r_1\delta r_2$ (δr_i is a bond displacement from equilibrium; p_i, the conjugate bond momentum; m_o, the mass of the O atom). As discussed in section II, the value of k_{intra} for DDA molecules can be estimated from the observed splitting between the symmetric and asymmetric stretch in the DDA band of crystalline octamer cubes near 3550 cm^{-1}; the splitting is similar to that of H_2O isolated in D_2O ice. The value of k_{intra} for DAA and DA molecules is much less important, because of the large frequency gap between the two bonds.. Thus, one can use reasonably safely the ice value ($k_{\text{intra}} = 0.0385$ mdyn/Å[54]) for all cluster molecules. Instead, a formula was adopted $k_{\text{intra}} = -0.110 + 0.07425\ (f_1 + f_2)$; $f_i = [\exp(x_i) - \exp(-x_i)]/[\exp(x_i) + \exp(-x_i)]$; $x_i = 0.015(3720 - \omega_i)$ where ω_i is the bond frequency in cm^{-1} calculated as described in the next subsection and the resulting k_{intra} is in mdyn/Å. This formula extrapolates smoothly between the gaseous value of the coupling (−0.11 mdyn/Å) and the ice one for DDA and employs the suggestion of a low-level ab initio calculation,[7] that the DAA value is closer to the gas phase than the DDA one.

The intermolecular coupling is modeled as an oscillating dipole−dipole interaction, $k_{dd}\delta r_1\delta r_2$, with $k_{dd} = \mu'^2[(e_1e_2) - 3(e_1e_r)(e_2e_r)]/r^3$, where e_1, e_2, and e_r denote unit vectors along the two bonds and along the distance vector r, calculated here using the minimum geometry. That is, the effect of intermolecular ZPM on the coupling was not included. (However, the largest coupling elements are only a few tens of inverse centimeters, while the pertinent spectral range is 800 cm^{-1}; therefore, this approximation should not affect the spectra significantly.) The OH bond dipole derivative is known to increase strongly with the strength of the hydrogen bond (or the red-shift in the OH frequency). Following combined ab initio and Monte Carlo results of ref 65 for liquid water and our studies of ice surface spectra,[54] linear dependence was adopted for $(\mu')^2$ on the bond frequency $\mu' = [0.464 + 0.03103(3720 - \omega_i)]^{1/2}$ where the result is in in D/Å; this formula yields the gaseous value $\mu' = 0.68$ D/Å[82] at the dangling OH frequency while at 3220 cm^{-1} (near the peak of the ice spectrum, see Figure 6), $\mu_i' = 4$D/Å, in accord with the value proposed for ice in ref 83. In the large distance limit, the exact choice of the origin of the dipole−dipole interaction (e.g., at the O atom, or at the OH midpoint) does not affect significantly the coupling. However, since the dipole−dipole interaction formula is used also for the nearest neighbor coupling, some choices should work better than others. A recent theoretical study of ice spectroscopy[84] suggested that the optimal choice is a point on the OH bond, 0.65 Å from the O atom; this choice is employed in the present study.

The Morse matrix elements $\langle 0|p_i|1\rangle$ and $\langle 0|\delta r_i|1\rangle$, which are needed in the calculation of the Hamiltonian matrix in the exciton basis, are given in ref 85. The infrared absorption intensity to an excited state[81] is proportional to $I = (E_{\text{exc}} - E_{\text{gs}})|\upsilon|^2$, where E_{exc} and E_{gs}, denote excited and ground state energies and the body-fixed components $k = x, y, z$ of the transition dipole vector υ are calculated *as* $\upsilon_k = \sum_i c_i e_{ik}\mu_i'\langle 0|\delta r_i|1\rangle$. Thus, the bond dipole derivative is assumed to be directed along an OH bond. In reality, this is true for ice; whereas in a gaseous water molecule, the bond derivative is directed 25.2° outside the bond.[57] The true orientation of the bond dipole derivatives in water clusters is an interesting (unanswered) question.

At present, no effort was made to calculate the line widths, which, experimentally, are typically in the range 10−25 cm^{-1}. To facilitate visual comparison with experiment, the calculated spectral lines were converted to Lorentzians of width 10 cm^{-1} (see Figure 8). Additional details on the computational model can be found in refs 54, 59, 79, 84. Note that the model does not include the effect of the Fermi resonance with the bending overtone. As further discussed below, we believe that this effect is small.

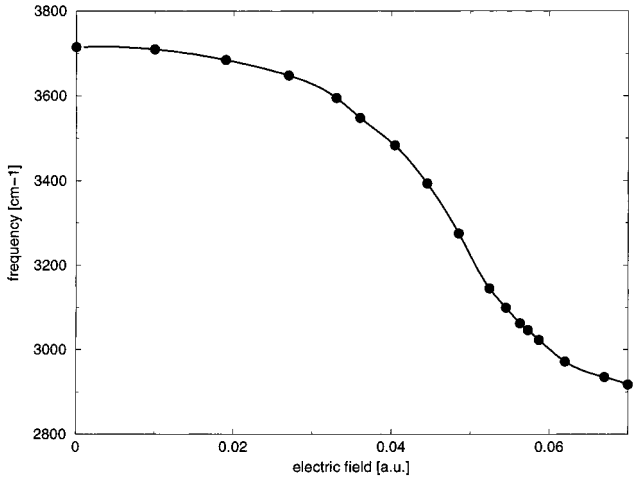

Figure 9. The function $\omega(E_{||})$. Cubic spline interpolation is used between the points.

3. Dependence of the OH Morse Parameters on the Hydrogen Bond Strength and on Intermolecular ZPM. As noted above, it is assumed here that the bond frequency ω_i is *some* function of $E_{||}$. The question to be addressed is whether one can reproduce the measured spectra with this parameterization. The function $\omega(E_{||})$, shown in Figure 9, was constructed by fitting to experiment, mostly to the $n = 7-8$ spectra. The function was represented as a sequence of points, with cubic spline interpolation between them. In this section it is explained how this function was used to obtain the bond force constant, while including ZPM effects.

The relation between OH stretch and intermolecular motion was assumed SCF-like. That is, the bond stretch constant $k_{\text{bond}} = M_{\text{OH}}[\omega(E_{||})]^2$ (M_{OH} is the reduced mass of O and H) was averaged over the intermolecular motion. First, energy minimization and normal mode analysis were carried out using EMP(fl). For the purpose of averaging, the intermolecular vibrational wave function was approximated as a product of Gaussians (i.e., harmonic ground state wave functions). Here, k_{bond} can be expanded as

$$k_{\text{bond}} = k_{\text{min}} + \sum_l F_l(Q_l) + \sum_{m,n} G_{m,n}(Q_m, Q_n) + ...$$

where k_{min} is the value at the minimum, Q_l, Q_m, Q_n denote intermolecular normal modes, F_l is a function of a single normal mode, and higher terms describe simultaneous dependence on two or more modes. It is now assumed that the main contribution to the average value of k_{bond} originates from the first two terms, and the contribution of $G_{m,n}$ and higher terms is neglected. To justify that one may consider the Taylor expansion of k_{bond} in normal modes, then $F_l = a_1Q_l + a_2Q_l^2 + a_3Q_l^3...$ and $G_{m,n} = b_{11}Q_mQ_n + b_{12}Q_mQ_n^2 + b_{21}Q_m^2Q_n + ...$ All low order terms in $G_{m,n}$ contain odd powers of Q_m, Q_n. If the intermolecular motion is not strongly anharmonic, then their average is small; whereas in F_l all even diagonal terms, starting from $a_2Q_l^2$, contribute to the mean value of F_l. Within these assumptions, the mean value of k_{bond}, averaged over ZPM, is given by

$$\langle k_{\text{bond}} \rangle = k_{\text{min}} + \sum_l \langle \Delta_l \rangle$$

$$\langle \Delta_l \rangle = \langle k_{\text{bond}}(E_{||}) - k_{\text{min}} \rangle_l$$

where the last average $\langle\ \rangle_l$ is over the lth Gaussian, while all other normal modes are set to zero. The latter averaging is carried out numerically, using four-point Gauss−Hermite integration.[86] The above procedure yields the bond force constant; the corresponding bond frequency is $\omega_i' = (\langle k_{\text{bond}} \rangle / M_{\text{OH}})^{1/2}$. However, for OH bonds it is preferable to use a Morse potential,[25,87] $D_i[1 - \exp(-\alpha_i \delta r_i)]^2$, rather than harmonic formulas. The free OH Morse parameters were taken as $D_o = 0.19036$ Hartree and $\alpha_o = 1.19801$ bohr^{-1}. For each bond i, these parameters were rescaled, so that the fundamental Morse frequency ω_i (i.e., the difference between the first two Morse energy levels divided by $\hbar$) will be equal to ω_i', calculated as described above.[88] The rescaled D_i and α_i were then used in the Morse matrix elements needed in the calculation.

It is of interest to compare the EMP spectra calculated without ZPM averaging (Figure 7), with ab initio spectra (Figure 5); the latter were also obtained for the minimum configurations, but by normal mode analysis. The crystalline three-band spectra ($O(S_4)_{\text{same}}$, $O(D_{2d})_{\text{opp}}$, N_{opp}, D_{bfl}) are qualitatively similar in both methods. Both methods yielded amorphous spectra with numerous peaks for the remaining clusters; however, despite vague similarities in the overall appearance of the spectra, the spacings between the peaks do not match.

4. Calculations of ZPE Contributions to the Binding Energy. In one set of calculations, the rigid body diffusion Monte Carlo method (RBDMC[89]) was employed, in conjunction with the rigid EMP potential. These calculations yielded intermolecular zero-point energy, $\text{ZPE}_{\text{inter}}$, in the framework of the rigid H_2O model. DMC is a numerical method to solve the time-independent Schrödinger equation by a random walk of a cloud of replicas of a quantum system;[90] in the long time limit the distribution of replicas in space approaches the vibrational wave function. The rigid body DMC treatment developed in our group[89] reduces the problem of numerical noise and allows for larger Monte Carlo steps; it is justified by the large gap between the inter- and intramolecular frequencies. The present calculations employed 2000 replicas, a time step of 30 a.u., and 10000−15000 steps per simulation. The value of $\text{ZPE}_{\text{inter}}$ seems converged within 0.1 kcal/mol.

In the second set, effects of molecular flexibility were included. The binding energy D_0 was calculated as a sum of minimum energy obtained with EMP(fl), plus $\text{ZPE}_{\text{inter}}$, plus $\Delta(\text{ZPE})_{\text{intra}}$. The value of $\text{ZPE}_{\text{inter}}$ was taken from the RBDMC simulation as described above. In order to double check this value, it was recalculated as a sum of harmonic zero-point energies of intermolecular normal modes, obtained from normal mode analysis employing EMP(fl). The two numbers for $\text{ZPE}_{\text{inter}}$, which are of the order of 3 kcal/mol/H_2O, differed by at most 0.14 kcal/mol/H_2O for the small cluster sizes; the difference decreased to a few hundredths kcal/mol/H_2O for $n = 10$.

$\Delta(\text{ZPE})_{\text{intra}}$ is a difference between the intramolecular ZPE in a cluster and in free H_2O. The main contribution to $\Delta(\text{ZPE})_{\text{intra}}$, originating from the stretching vibrations, was calculated as a difference between Morse ground state energies of OH bonds in a cluster and free OH. The small bending contribution was estimated as $0.5\hbar(\omega_{\text{cluster}} - \omega_{\text{gas}}) \approx 0.1$ kcal/mol/H_2O. (The gas bending frequency is 1595 cm^{-1}; the bending frequency in the cluster was taken as 1668 cm^{-1}, the mean of the DDA and DAA frequencies measured for the ice surface.[87,91])

B. Results: Cluster Energetics Calculated with Ab Initio and EMP. Table 2 gives the listing of cluster energies both in ab initio and EMP. Figure 10 shows the results for for the minimum energy D_e/n, and for the binding energy corrected for ZPE D_0/n, in units of kcal/mol/H_2O (ab initio values were corrected for BSSE and deformation). While the numerical values obtained in the different methods of calculation differ

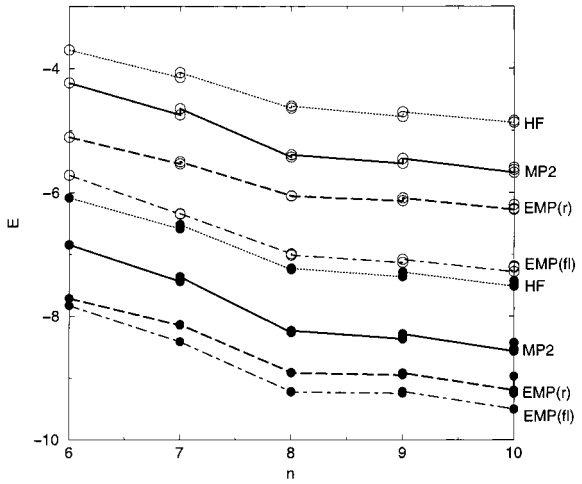

Figure 10. Variation of the minimum energy D_e/n (bottom four curves) and the binding energy D_0/n (top four curves), with the cluster size. Energies are in kcal/mol/H_2O. All 10 structures were included in the plot in the same order as in Table 2.

from each other, the trends as a function of n are quite similar. The cluster energy decreases by about 1 kcal/mol/H_2O between $n = 6$ and $n = 8$, and by only 0.2−0.3 kcal/mol/H_2O in the range $n = 8-10$. The following additional points are of interest.

a. At the present level of ab initio, the correlation (estimated as a difference D_e(MP2) − D_e(SCF)) contributes about −1 kcal/mol/H_2O (11−12%) to the binding energy. The ranges cited here and below refer to the variation between $n = 6$ to $n = 10$; i.e., the correlation contribution increases from 11% for $n = 6$, to 12% for $n = 10$.

b. The MP2 minimum energy D_e/n is higher by 13−9% (about 1 kcal/mol) than the EMP(fl) value; the difference is somewhat smaller for EMP(r). The minimum energies calculated with MP2 tend to be too high, as a result of incomplete inclusion of correlation. The EMP binding energy of ice is very close to the value derived from experiment;[61] however, this potential may overestimate the dimer well depth by as much as 10%.[92] Thus a several percent overestimate for the $n = 6-10$ clusters is not unlikely. The true D_e/n lies probably somewhere between the MP2 and EMP values.

c. While the energy trends as a function of n seem quite similar in all the different methods, the small energy differences between the different isomers vary and do not seem to be very reliable in any of the methods. The pertinent differences are up to several hundredths' of kcal/mol/H_2O. For example, the energies of the "opp" isomers of $n = 8$ and $n = 10$ are lower than those of the "same" isomers in MP2, but higher in EMP(fl). The calculated ZPE-corrected energy of D_{bfl} is 0.08 kcal/mol/H_2O above that of the lowest double-pentameric isomer, both in MP2 and EMP(fl); however, the experiment suggests that D_{bfl} is the ground state configuration.[51]

d. The cluster energy cannot be considered as a simple sum of bond energies. For example, the lowest energy nonamer differs from the $O(D_{2d})_{opp}$ octamer by an addition of a *two*-coordinated water molecule to a wholly three-coordinated cluster; despite that, the mean binding energy per molecule *decreases* slightly from $n = 8$ to $n = 9$. The same is true, more dramatically, for the transition from $n = 6$ to $n = 7$. Also, D_{same} and D_{opp} decamers include two extra hydrogen bonds, with respect to D_{bfl}. Despite that, the minimum energy of D_{same} and D_{opp} is lower by only 1 kcal/mol (MP2), or 2.5 kcal/mol (EMP(fl)), as compared to D_{bfl}.

e. While the minimum energy per molecule decreases substantially in the range $n = 6-10$, the fractional contributions

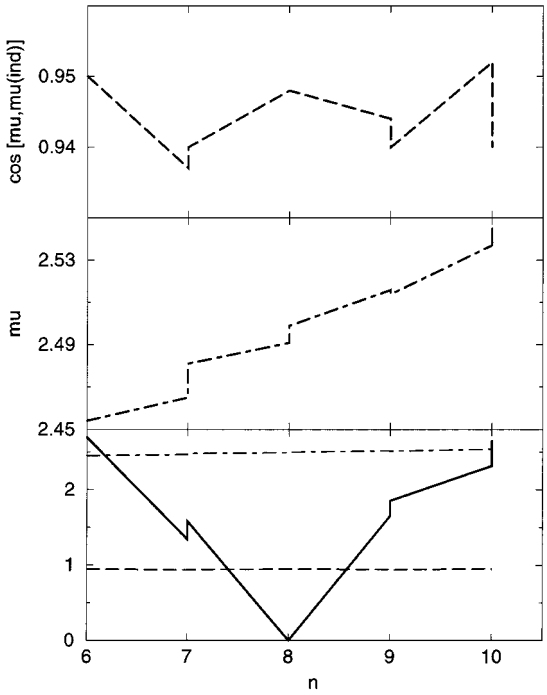

Figure 11. Solid: cluster dipole, in Debye. Dot-dashed: mean molecular dipole, in Debye. Dashed: mean cosine of the angle between the total molecular dipole, and the induced dipole. The last two quantities are shown in the top panels, on an expanded scale. All 10 structures were included in the plot in the same order as in Table 2. EMP(r) calculation.

of the different energy components remain strikingly constant. The nearly constant fractional contribution of correlation to ab initio binding energies was mentioned above. The same kind of effect is seen in EMP calculations. For EMP(r), the fractional contribution to minimum energy of many body terms due to polarizability is in the range 22−24.5%. The intermolecular ZPE is in the range 34−31% of $|D_e|$ for EMP(r), and 27−22% for EMP(fl).

f. A non-negligible contribution to the binding energy (between −0.6 and −0.8 kcal/mol/H_2O) originates from the stretch ZPE. The stretch frequency is lowered substantially as a result of hydrogen bonding, resulting in additional cluster stabilization with respect to gaseous H_2O.

g. The total ZPE calculated with MP2 is 20−40% larger than that obtained with EMP(fl). This rather large difference seems to be due, predominantly, to the difference in the shape of the potential wells in the two schemes. (As noted above, MP2 frequencies were calculated for the BSSE uncorrected ab initio potential.)

C. Cluster and Molecular Dipoles. the results pertaining to the dipoles are shown in Figure 11. The pertinent calculations were carried out for minimum energy configurations obtained with EMP(r). (The results with EMP(fl) are very similar, except that the nonzero dipole sizes are larger by a few hundredths of Debye.)

Hydrogen bonding is known to enhance molecular dipoles of H_2O in clusters and condensed phases.[93,94] The mean molecular dipoles in the clusters increase slightly as a function of n, from 2.45 to 2.55 Debye. These values are still quite short of 2.81 Debye, obtained for proton disordered ice at a minimum energy configuration, with the same potential.[61] Interestingly, in the clusters, the induced molecular dipole, and the total H_2O dipole are not aligned; the mean cosine of the angle between

the two vectors (0.945) corresponds to misalignment of about 19°. (The mean cosine obtained in a 20 K simulation of ice is 0.999.)

The total cluster dipole varies strongly as a function of *n*. The largest values, corresponding to $n = 6$ (Hx_{prism}) and $n = 10$ (D_{bfl}) are 2.7 Debye, close to the mean H_2O dipole. A minimum is obtained for the zero-dipole octamers.

D. Intermolecular ZPM Effect on OH Stretch Spectra. Figures 7 and 8 show OH stretch spectra calculated within the EMP scheme, without and with the ZPM correction. The effect of ZPM is complicated. Deviation of a hydrogen bond from linearity and hydrogen bond stretching reduce $E_{||}$ and thus increase the bond frequency. However, there is also a contribution from short bond length configurations with high $E_{||}$. The bond force constant does not depend linearly on intermolecular displacements from equilibrium (if it did, the calculated effect were zero). ZPM correction is exceedingly sensitive to the detailed shape of the $\omega(E_{||})$ function; in fact, this function was constructed by laborious adjustment of the points in Figure 9, to obtain reasonable agreement with experiment for $n = 7, 8$. The calculated ZPM effect varies from bond to bond; for hydrogen bonded OH, the frequency shifts due to ZPM are mostly several tens of inverse centimeters. The shifts may be either positive or negative; all frequency shifts below 3350 cm^{-1} are positive, while both positive and negative shifts are found in the higher frequency range. Negative shifts were found only for $n = 6, 7, 10$ (D_{same} and D_{opp}). Some of the positive shifts in the low frequency range are as large as 80−200 cm^{-1}.

Comparison of Figures 7 and 8 shows that the main ZPM effect on the relatively simple crystalline spectra ($O(S_4)_{same}$, $O(D_{2d})_{opp}$, N_{opp}, D_{bfl}) is a blue-shift of the DAA band, otherwise the qualitative appearance of the spectra is preserved. However, the complex pattern of peaks of the amorphous clusters is altered significantly by the ZPM, chiefly because of nonuniform shifts of the different peaks. Note in particular the changes in the $n = 7$ spectra and the large blue-shift of the middle feature of D_{opp}, D_{same} (from 3200 to 3340 cm^{-1}). While the present numerical results depend on the parameterization used in this study, the main qualitative result, that the ZPM effects may alter substantially the spectra, is likely to be correct.[25]

E. Calculated Versus Experimental OH Stretch Spectra. The level of agreement with experiment which could be achieved with the present scheme is seen from comparison of Figures 6 and 8. The comparison between theory and experiment is associated with several difficulties. The chief one is that we are using theory for assignment, and at the same time trying to learn something about the molecular force field, using the experimental data. As noted above, the calculated small energy differences between different isomers, which are of an order of several hundredths kcal/mol/H_2O ($\leq$1 kcal/mol = 500K), are not likely to be very meaningful in any of the computational methods. On the other hand, the estimated temperature of the clusters is in the range 60−120 K, and therefore the experimental conditions discriminate between structures differing in energy by a fraction of a kcal/mol. Thus, the calculated low energy minima should be considered as *candidates* for the observed structures; the final assignment can be suggested only by comparison of observed and calculated spectra. Moreover, the list of candidates may be incomplete, since even thousands of minimizations starting from random initial conditions are not guaranteed to produce all of the low lying minima. The considerations used to assign the spectra to the different structures can be found in refs 51 and 53, and are also reviewed below, together with the discrepancies between theory and experiment. The main discrepancies pertain to intensities and to missing spectral lines in the calculated spectra.

1. Octamers. Here, the assignment presents the least difficulty; all of the peaks in the spectrum are reproduced quite well using the two $O(S_4)_{same}$ and $O(D_{2d})_{opp}$ structures. These structures were suggested in the past as the lowest $n = 8$ minima (see, e.g., refs 33, 36, 28) and were also obtained by us as the lowest minima in numerous minimizations employing EMP. Moreover, all calculations apparently agree that these two minima are particularly stable and close in energy to each other. Each of the two peaks below 3100 cm^{-1} is contributed by a different isomer, while the doublet near 3550 cm^{-1} is due to symmetric−antisymmetric stretch splitting in DDA molecules of both isomers. The latter splitting is not due entirely to intramolecular coupling; when the latter is set to zero, the splitting is reduced but does not disappear.

The calculated intensity of the dangling OH band above 3700 cm^{-1} is well below that of hydrogen bonded bands, while the measured peak intensity of all three bands is similar. A similar discrepancy was found for other cluster sizes as well, and in ab initio. One may note that, in the experiment, the infrared transition probability is weighted by the dissociation probability and that there may be a problem of line saturation. On the other hand, our modeling efforts are hampered by the lack of information on detailed dependence of the direction and the size of bond dipole derivative on hydrogen bond strength and geometry (see section III-2 above).

2. Heptamers. As noted in the ab initio section, the assignment to two lowest energy isomers is supported by two lines measured below 3000 cm^{-1}; each isomer contributes one low frequency feature. The different spectral features are reproduced by the calculation within several tens of inverse centimeters. The assignment of the observed peaks to the different OH bonds of the heptamers can be found in ref 53.

The main discrepancy is in the number of peaks. In the DAA band near 3100 cm^{-1} there are three calculated peaks; the measured band looks more congested. Similar observations are made in the 3500−3600 cm^{-1} DDA band, although here the discrepancy is smaller.

We tried unsuccessfully to improve the agreement by adding additional low energy $n = 7$ isomers, some of which are described in ref 53. A possible explanation might be some contamination by the octamers, whose spectral lines are about 3.5 times more intense than the heptamer ones. (Note the differences in the intensity scale of $n = 7$ and $n = 8$ in Figure 8, which are due to the fact that heptamer peaks are contributed by individual bonds, while the octamer peaks originate from collective modes.) The heptamer was investigated by a number of theoretical studies;[13,16,21,26,27,33,32] some of them[13,26,33,32] obtained the same lowest minimum (or two minima) as in this study.

3. Nonamers. The N_{opp} isomer corresponds to the lowest energy in both EMP and MP2; it was also proposed as the lowest energy structure in a number of other studies.[16,26,31,32,38] Its calculated spectrum includes a doublet in the DDA region, in accord with experiment, and two dominant peaks in the low frequency band; one at 3077 cm^{-1}, due to collective cage excitation, and another at 3137 cm^{-1}, due to collective vibration of the DA molecule, and the adjacent DAA molecule that points toward it (see Figure 2). The features match reasonably the experiment; however, the experimental band near 3100 cm^{-1} is continuous and includes several overlapping peaks, rather than two isolated ones. The next nonamer isomer, N_{same}, has a rather different spectrum, with features in the 2900−3000 cm^{-1} and

3400−3500 cm^{-1} regions. Interestingly, in this isomer, the DA frequency is much higher than that in N_{opp}, close to DDA. The features in the 3400−3500 cm^{-1} range are due mostly to the collective excitation of the hydrogen bonded OH in the DA molecule and of the adjacent DDA which is pointing toward it (see Figure 2, a similar result was obtained in ab initio). Unfortunately, in the pertinent set of measurements, the range below 3000 cm^{-1} was not explored. There seem to be no peaks in the 3400−3500 cm^{-1} range, which however was only partially accessible to the experiment (see Appendix). So the second isomer cannot be ruled out at present, but it does not seem to account for the missing lines in the 3100 cm^{-1} band. The peak intensity of the nonamer lines is comparable to that of $n = 8$, 10, therefore the extra lines do not seem to be due to contamination. The same problem is encountered for $n = 10$; possible explanations are discussed later in this section.

4. Decamers. The two D_{opp}, D_{same} isomers correspond to the lowest energy structures, obtained as a result of numerous minimizations employing EMP. The calculated spectra of the two isomers nearly overlap (the doublet structures of the three features below 3400 cm^{-1} originate from contributions from two isomers). The new structural feature with respect to $n = 8$, 9 is the symmetric DDA−DDA and DAA−DAA bonding in one of the walls of the cage, the result of the odd number of molecules in the pentamer rings (see back walls of the two minima in Figure 3). The result is a peak in the 3300−3400 cm^{-1} range corresponding to a collective excitation of two nearly parallel bonds connecting the DDA−DDA and DAA−DAA pairs. This spectral feature is absent in the experiment. Better agreement with experimental spectra was attained using the D_{bfl} isomer, whose calculated minimum energy is higher than that of the lowest energy double pentamer (by 1.4 kcal/mol in MP2 and by 2.6 kcal/mol in EMP(fl)). The energy difference is reduced substantially after inclusion of ZPE effects (to 0.8 kcal/mol in both methods); the reduction is due to greater rigidity of the D_{opp}, D_{same} structures. D_{bfl} is still higher in energy; however, errors in energy differences of an order of 1% of minimum energy are not unexpected, so in reality D_{bfl} could be the ground state. One may note that D_{same} was obtained in ref 32 as the lowest decamer minimum in the TIP4P potential, while ref 31 proposed D_{bfl} as the lowest TIP3P minimum.

As in the case of the nonamer, the calculated low frequency band of D_{bfl} includes two peaks, rather than several overlapping peaks, as in the experiment. We did not succeed in finding another isomer with a spectrum that is similar to D_{bfl}, except for displaced low frequency lines, to account for this discrepancy. In the course of the search, a cis isomer of D_{bfl} was found, in which the dangling OH of the two DA molecules points to the same side of the cluster rather than to two opposite sides (see Figure 2 and further discussion below); however, the calculated spectra of the two isomers virtually overlap.

5. Missing Lines in the Low Frequency Band of n = 9, 10. One possible mechanism to account for the missing lines is a Fermi resonance with the bending overtone. This possibility was discarded on the following grounds. The origin of the bending overtone in the gas phase is at 3152 cm^{-1}. A recent study[91] of the ice surface spectroscopy provides the values 1684 and 1652 cm^{-1} as bending fundamentals of DDA and DAA molecules, 89 and 57 cm^{-1} above the gaseous bending frequency. The calculated MP2 bending frequencies in clusters are at least 80 cm^{-1} above the gas phase. Therefore, the bending overtone frequencies in the clusters are expected more than 100 cm^{-1} above the gas phase, well beyond the upper frequency limit (about 3150 cm^{-1}) of the problematic DAA/DA band. In fact, a small peak measured in the heptamer at 3250 cm^{-1} was assigned by us as a bending overtone.[53]

Another possibility is hot bands, that is, OH stretch excitations in clusters with excited intermolecular modes. Several lowest normal frequencies, corresponding to skeletal O··O··O bending, are in the 45−90 cm^{-1} range both in MP2 and in EMP. Therefore, there should be a substantial component of such excited states, if the cluster temperature is near the estimated upper limit of 120 K. The OH line shifts resulting from such excitations can be estimated in the framework of the present scheme. The shifts are at most 20 cm^{-1} and are insufficient to account for the observed continuous band width of about 100 cm^{-1}.

Of course, our minimization studies could have missed some additional structures which contribute the missing lines.

Finally, the possibility of splittings due to multiple minima is considered. The present scheme assumes a cluster localized around a single minimum and performing approximately harmonic intermolecular ZPM. This picture is supported by the fact that intermolecular ZPE calculated with RBDMC is reproduced within several percent or better while using the harmonic normal modes. On the other hand, clusters have, by definition, multiple minima obtained by permutations of water molecules. We found however that the intermolecular connectivity network of the cluster is retained throughout rather lengthy DMC runs; therefore, exchange of molecules seems infrequent, and the corresponding tunneling splittings, small. However, in the case of N_{opp}, N_{same}, and D_{bfl}, DMC simulations were found to sample more than one minimum. Each of the nonamers frequents two minima, and D_{bfl} frequents four minima. The "loose" anharmonic degree of freedom, which connects the minima, corresponds to a hindered rotation of the dangling OH of each DA molecule; the orientation of the dangling OH in the corresponding minima differs by about 100 degrees. In the $n = 9$ isomers, as shown in Figure 3, the motion can be described as a transition from an "up" orientation to a nearly horizontal orientation. The two minima are exactly isoenergetic in N_{opp}, and nearly isoenergetic in N_{same} (the "up" orientation is 0.003 kcal/mol higher in energy for the EMP potential). In D_{bfl}, as shown in Figure 2, each of the two dangling OH of DA may point either "into the page" or "out of the page"; one then obtains two equivalent trans minima and two equivalent cis minima (in EMP, cis is 0.02 kcal/mol below the trans; the ab initio calculations described in this article pertain to trans, which was discovered first[95]). The fact, that all of the minima are frequented during the DMC simulation suggests a low transition barrier. The multiple well potential may support two or more low lying states, which, at the experimental temperature, could result in a complex DAA/DA spectral band. This effect cannot be reproduced in the framework of the present treatment of the effect of intermolecular motion on the spectra, which assumes delocalization around a single minimum. More investigation is necessary. Related high amplitude motions of DA molecules have been described for the hexamer cage.[41,46]

It is noted finally, that the remaining complexes were found in fact to be localized around their respective single minima throughout the DMC runs.[96]

IV. Some Comments on the Relation between Clusters and Condensed Phases

A question that is frequently asked by people outside the field is "What are clusters good for?" After all, a cluster is not a very important form of matter in nature. The obvious answer is that clusters constitute a valuable source of information on

intermolecular interactions. However, in addition it is often suggested that clusters can be used as small models for condensed phases. Then the question to be asked is "Which condensed phases?" It has been suggested that cluster studies are relevant to either liquid water or ice, on the basis of the evolution of H_2O properties toward condensed phases as a function of cluster size.

In fact, interesting analogies can be drawn between clusters and condensed phase behavior. For example, based on the R(O··O) distributions, one can divide the clusters into crystal-like and amorphous categories (see section IIC). Studies of cluster dynamics by other authors[27,28,97] showed interesting melting-like transition in water clusters of various sizes. Still, the clusters in the $n = 6-10$ size range are a very long way from any of the condensed phases (liquid water, crystalline, or amorphous ice). This can be seen, for example, from the fact that IR spectra of clusters are totally different from those of condensed phases (Figure 6); the latter peak within the spectral gap of the $n = 8-10$ clusters. The difference is not surprising, since the structure of all these condensed phases is dominated by four-coordinated water molecules, while the structure of the pertinent clusters is dominated by three-coordinated ones. The spectrum of the heptamers includes peaks within the gap, the result of the presence of a broad range of hydrogen bonding geometries; still, the heptamers lack totally the dominant condensed phase species—a water molecule with four bonds in an approximately tetrahedral arrangement. *As long as this species is absent, a water cluster is neither a model for liquid nor for ice in their macroscopic forms.* Characteristic features of $(H_2O)_n$ in the size range of our interest, the presence of two distinct kinds of molecules (DDA and DAA) and three kinds of OH bonds (DAA, DDA, and dangling), also set clusters apart from condensed phases. One may note that clusters can be considered a high-density form of H_2O, as compared to ordinary condensed phases. For example, the ice Ih structure is dominated by hexagonal rings of water molecules with much empty space in between, while in the clusters considered here, the typical ring size is of 3−5 water molecules.

The condensed phase which is most closely related to the clusters is the surface. (The clusters are "all surface".) The spectrum of the ice surface, obtained by Devlin[73] is shown in Figure 6. While infrared intensity is present in the low and high frequency range characteristic of cluster DAA and DDA, the surface spectra are still quite different from the cluster ones. This finding is not too surprising. The surface bilayer of ice includes more than 50% of four-coordinated water molecules.[54] Moreover, the surface three-coordinated molecules are connected to four-coordinated H_2O, rather than to other three-coordinated molecules, as in the clusters, and the surface DDA bonds are expected to be much less strained.

The final comment pertains to proton disorder in crystalline ice and its relation to clusters. Ordinary ice Ih and some other ice forms are proton disordered.[94] That is, molecular orientations are random within the constraints of the so-called ice rules (two chemically-bonded and two hydrogen-bonded H atoms around each O, in a tetrahedral arrangement). Thus only O atoms form a periodic arrangement, while H atoms are disordered. A partial transition of ice Ih to the ordered ferroelectric form can be induced at 72 K, in the presence of the KOH impurity.[80] The small $n = 8-10$ crystallites detected in the beam experiment[51] are "proton-ordered" in a sense that only a few low energy H-atom arrangements are present. However, minimizations employing EMP resulted in numerous additional minima, which can be divided into families, characterized by a similar O-atom arrangement and different H-atom arrangements. (Related issues are addressed in ref 98 in the context of neutral and protonated water clusters.) All of the minima shown in Figures 1−3 have numerous higher energy "cousins" of a similar O-atom structure. As already noted in ref 51, the higher minima are characterized by broadening and overlap of DDA and DAA bands, i.e., an amorphous spectral signature. (The broadening is due to DDA−DDA and DAA−DAA bonds and to asymmetry of the structures.) As crystalline clusters are heated, broadening of spectra should occur as a result of orientational disordering, transitions between different "prototype" O-atom arrangements, and, ultimately, melting. Investigation of the interplay between the different factors is of interest. Broadening as a function of temperature should be observable experimentally.

V. Summary

The present study considered the structural, energetic, and spectroscopic trends in three-dimensional water clusters from $n = 6$ to $n = 10$. The MP2 (frozen core)/DZ1P calculations are reported, together with studies employing a polarizable empirical potential. The chief observable of our interest is the OH stretch spectrum, because of its striking sensitivity to hydrogen bonding. The ten studied structures are shown in Figures 1−3; most of them were used to assign the recently measured OH stretch spectra of size selected water clusters.[51,53] The structures may be considered as derived from octamer cubes by either insertion or removal of water molecules.

The structures can be loosely divided into crystal-like ($O(S_4)_{same}$, $O(D_{2d})_{opp}$, N_{opp}, D_{bfl}) and amorphous (Hx_{prism}, H_{low}, H_{nxt}, D_{opp}, D_{same}) groups; N_{same} is an intermediate case. The main form of hydrogen bonding in the first group is asymmetric, between DDA and DAA three-coordinated water molecules; all bonds emanating from DDA are long, and all bonds emanating from DAA are short. All O··O bonds in the same group are of similar length (at 2.62 and 2.79 Å in MP2). The amorphous structures include, in addition, symmetric bonds between the same kinds of molecules (DDA−DDA and DAA−DAA). The small amorphous clusters include strained 3-membered rings. The result is a broad distribution of nearest neighbor O··O distances, rather than two peaks.

The O··O nearest neighbor distance distribution is mimicked by the OH stretch spectra. The crystal-like structures yield two distinct relatively narrow spectral features in the hydrogen-bonded region corresponding to DDA and DAA bonds, with a gap in between. The amorphous structures yield numerous hydrogen bonded bands in a broad spectral range. This result is in qualitative accord with the experimental spectra. The rescaled DDA/DAA frequencies calculated on the MP2 level for the crystal-like clusters correspond to mean frequencies near 3520/3150 cm^{-1}, in not unreasonable agreement with experimental values near 3550/3070 cm^{-1}. Another experimental result reproduced by the ab initio calculations, is the remarkably broad frequency range (around 800 cm^{-1}) covered by the heptamer spectrum. However the ab initio calculations at the present level are insufficient to reproduce the finer features of the spectra, such as the symmetric−antisymmetric stretch splitting of the DDA band in the octamer spectrum and the intricate seven band peak pattern of the heptamers.

An effort was then made to construct an empirical model capable of reproducing the experiment. For each structure, OH stretch excitations were calculated by diagonalizing a Hamiltonian matrix in an exciton basis. The OH bonds were treated as coupled local anharmonic oscillators. The connection between the bond frequency and the hydrogen bond strength was

modeled by assuming that the bond force constant is determined by $E_{||}$, the electric field component parallel to OH, at the H atom; this connection was suggested by past ab initio studies.[60] $E_{||}$ was calculated using permanent charges and induced dipoles of an empirical polarizable potential EMP. A continuously decreasing function $\omega(E_{||})$ was constructed (Figure 9), with which it was possible to reproduce the measured spectra of $n = 7-10$, within a few tens of inverse centimeters (see Figures 6 and 8). The main discrepancy is some "missing" lines for $n = 9, 10$ in the calculated spectra; the discrepancy may be caused by line splitting originating from double well vibration of two-coordinated DA molecules. It is hoped that, despite its limitations, the present scheme will be useful in the assignment of OH spectra of larger clusters and other water-containing systems. (It is presently implemented for ice surface spectroscopy.[54]) The calculations demonstrated high sensitivity of OH spectra to structural details and, in accord with some previous studies,[78,79] a substantial effect of intermolecular zero-point motion on intramolecular cluster spectra.

Cluster energetics was investigated using both ab initio and EMP. Despite the differences in MP2 and EMP energy values, there is good agreement in the trends as a function of n (see Figure 10). However, small energy differences between adjacent isomers for a given n do not agree and, more generally, do not seem very reliable in any of the currently available computational methods. The cluster energy cannot be considered a simple sum of hydrogen bond energies, because of substantial many body effects. For example, D_{same} and D_{opp} decamers include two extra hydrogen bonds with respect to D_{bfl}; however, the minimum energy difference is small, well below the value expected for two hydrogen bonds. The ZPE contribution to D_0 constitutes about 25% of the well depth and modifies significantly the cluster energetics. A non-negligible *negative* contribution to the binding energy originates from the stretch ZPE; this is because the stretch frequency is lowered substantially as a result of hydrogen bonding, resulting in additional cluster stabilization with respect to gaseous H_2O.

Finally, the relation was discussed between clusters in the present size range, and condensed H_2O phases. While interesting analogies can be drawn, the clusters are a long way from any of the macroscopic condensed phases, as long as the cluster structure is dominated by three- rather than four-coordinated water molecules. This point is exemplified, for example, by the totally different OH stretch spectra of clusters and of H_2O liquid and ice (see Figure 6).

Acknowledgment. We thank Devlin, J. P. for the unpublished figure of ice and ice surface spectra used in Figure 6 and for very helpful discussions. This work was supported by the Foundation of Chemical Research and the Polish Scientific Research Council (KBN), Grant No. 3 T09A 056 14 (J.S.), the Niedersachsen-Israel Programm der Volkswagenstiftung (V.B. and U.B.), and the Deutsche Forschungsgemeinschaft (U.B.). J.S. thanks ICM in the Warsaw University for computer time.

Supporting Information Available: Nine tables with unscaled ab initio frequencies and intensities for $n = 7-10$ for all of the isomers discussed in the article. This material is available free of charge via the Internet at http://pubs.acs.org.

Appendix: Experimental

Since the experiments are described in some detail in refs 51 and 53 and new results have not been obtained, we will give here only a short account of the methods applied. The clusters are prepared by an adiabatic expansion of a dilute mixture of water vapor at temperatures of 338 K to 360 K with helium as carrier gas at pressures of 1.8 bar to 2.3 bar. The nozzle is either a conical one (opening angle: $2\alpha = 30°$, diameter: 90 μm, length: 2 mm) for $n = 8, 9, 10$ or a plain one (diameter 146 μm) for $n = 7$. Then the clusters are size selected by momentum transfer in a scattering experiment with helium atoms. This technique has been developed in the laboratory of one of the authors in Göttingen[99,100] and allows selection of clusters up to sizes of about $n = 15$, provided that the angular and velocity resolutions of the apparatus are high enough to separate the different cluster contributions. This is mainly achieved by using helium in the production of the two beams. An important variable to characterize the clusters is the temperature. It sensitively depends on the conditions of the source and the beam composition. Unfortunately, it is difficult to measure it in a straightforward way. We are working on two methods. One is the simulation of the cluster production and the relaxation in the supersonic expansion. The other possibility is the determination from the deexcitation of low energy vibrational cluster modes in inelastic helium atom scattering experiments.[101] Both evaluations are under way, and first estimations give temperatures between 60 and 120 K.

The particles are detected by electron impact ionization and mass analyzed by a quadrupole mass filter. The detector is set on the largest possible scattering angle for each size. Clusters of larger size cannot reach this angle. To discriminate against the smaller clusters in the beam the mass spectrometer is operated at the masses of the corresponding nominal masses, the protonated $(H_2O)_nH^+$ ions.

Then the size selected cluster beam interacts with the tunable infrared radiation of an optical parametric oscillator pumped by a pulsed Nd:YAG laser. The tuning range is between 2400 and 3800 cm^{-1} at an average output energy of 2 mJ/pulse, a resolution of 0.2 cm^{-1}, and a repetition rate of 20 Hz. Because of water impurities in the crystal, the arrangement has an intensity gap between 3460 and 3500 cm^{-1}. In the accessible frequency range, the OH stretch mode of the water molecules is excited, and subsequently the clusters dissociate by vibrational predissociation. The decrease in the detector signal is used to record the spectrum as function of the laser frequency. What is plotted in Figure 6 are in fact dissociated fractions $P_{diss} = 1 - \exp[-\sigma(\upsilon)F/h\upsilon]$, where $\sigma(\nu)$ represents the dissociation cross section, F the laser fluence, and $h\upsilon$ the photon energy. Here, $\sigma(\nu)$ is, in turn, the product of the transition dipole moment and the decay profile of the dissociation.[102] Thus one cannot directly compare these results with calculated intensities which are only based on the transition dipole moment. In addition, the laser fluence is large enough that saturation effects cannot be excluded for those parts of the spectrum with large cross-sections, while parts with small cross-sections are not affected.

References and Notes

(1) Pimentel, G. *J. Chem Phys.* **1951**, *19*, 446.
(2) Fraser, G. T. *Inter. Rev. Phys. Chem.* **1991**, *10*, 189.
(3) Scheiner, S. *Ann. Rev. Phys. Chem.* **1994**, *45*, 23.
(4) Leforestier, C.; Braly, L. B.; Liu, K.; Elrod, M. J.; Saykally, R. J. *J. Chem. Phys.* **1997**, *106*, 8527.
(5) Chalasinski, G.; Szczesniak, M. M.; Cieplak, P.; Scheiner, S. *J. Chem. Phys.* **1991**, *94*, 2873.
(6) Gonzalez, L.; Mo, O.; Yanez, M.; Elguero, J. *J. Mol. Struct. (Theochem)* **1996**, *371*, 1.
(7) Knochenmuss, R.; Leutwyler, S. *J. Chem. Phys.* **1992**, *96*, 5233.
(8) Xantheas, S. S.; Dunning, T. H. *J. Chem. Phys.* **1993**, *99*, 8774.
(9) Van Duijneveldt-van de Rijdt, J. G. C. M.; van Duijneveldt, F. B. *Chem. Phys.* **1993**, *175*, 271; *Chem. Phys. Lett.* **1995**, *237*, 560.
(10) Wales, D. J.; Walsh, T. R. *J. Chem. Phys.* **1997**, *106*, 7193.
(11) Kim, K.; Kim, K. S. *J. Chem. Phys.* **1998**, *109*, 5886.
(12) Kim, J.; Mhin, J.; Lee, S. J.; Kim, K. S. *Chem. Phys. Lett.* **1994**, *219*, 243.

(13) Kim, J.; Mujumdar, D.; Lee, H. M.; Kim, K. S. *J. Chem. Phys.*, in press.
(14) Tsai, C. J.; Jordan, K. D. *Chem. Phys. Lett.* **1993**, *213*, 181.
(15) Kim, K.; Jordan, K. D.; Zwier, T. S. *J. Am. Chem. Soc.* **1994**, *116*, 11568.
(16) Jensen, J. O.; Krishnan, P. N.; Burke, L. A. *Chem. Phys. Lett.* **1995**, *241*, 253; **1995**, *246*, 13; **1996**, *260*, 499.
(17) Xanteas, S. S. *J. Chem. Phys.* **1994**, *100*, 7523; **1995**, *102*, 4505.
(18) Fowler, J. E.; Schaefer, H. F. *J. Am. Chem. Soc.* **1995**, *117*, 446.
(19) Kahn, A. *J. Phys. Chem.* **1995**, *99*, 12450.
(20) Estrin, D. A.; Paglieri, L.; Corongiu, G.; Clementi, E. *J. Phys. Chem.* **1996**, *100*, 8701.
(21) Kryachko, E. S. *Chem. Phys. Lett.* **1997**, *272*, 132.
(22) Guiang, C. S.; Wyatt, R. E. *Int. J. Quantum Chem.* **1998**, *68*, 233.
(23) Jiang, J. C.; Chang, J. C.; Wang, B. C.; Lin, S. H.; Lee, Y. T.; Chang, H. C. *Chem. Phys. Lett.* **1998**, *289*, 373.
(24) Stillinger, F. H.; David, C. W. *J. Chem. Phys.* **1980**, *73*, 3384.
(25) Reimers, J. R.; Watts, R. O. *Chem. Phys.* **1984**, *85*, 83.
(26) Pillardy, J.; Olszewski, K. A.; Piela, L. *J. Mol. Struct. (Theochem)* **1992**, *270*, 277.
(27) Farantos, S. C.; Kapetanikis, S.; Vegiri, A. *J. Phys. Chem.* **1993**, *97*, 12158.
(28) [28] Wales, D. J.; Ohmine, I. *J. Chem. Phys.* **1993**, *98*, 7245; **1993**, *98*, 7257.
(29) Sremaniak, L. S.; Perera, L.; Berkowitz, M. L. *J. Chem. Phys.* **1996**, *105*, 3715.
(30) Jung, J. O.; Gerber, R. B. *J. Chem. Phys.* **1996**, *105*, 10332.
(31) Niesse, J. A.; Mayne, H. R. *J. Comput. Chem.* **1997**, *18*, 1233.
(32) Wales, D. J.; Hodges, M. P. *Chem. Phys. Lett.* **1998**, *286*, 65.
(33) Kim, K. S.; Dupuis, M.; Kie, G. C.; Clementi, E. *Chem. Phys. Lett.* **1986**, *131*, 451.
(34) Dykstra, C. E. *J. Chem. Phys.* **1989**, *91*, 6472. Franken, K. A.; Jalaie, M.; Dykstra, C. E. *Chem. Phys. Lett.* **1992**, *198*, 59.
(35) Sabo, D.; Bacic, Z.; Bürgi, T.; Leutwyler, S. *Chem. Phys. Lett.* **1995**, *244*, 283.
(36) Tsai, C. J.; Jordan, K. D. *J. Chem. Phys.* **1991**, *95*, 3850.
(37) Tsai, C. J.; Jordan, K. D. *J. Phys. Chem.* **1993**, *97*, 5208.
(38) Lee, C.; Chen. H.; Fitzgerald, G. *J. Chem. Phys.* **1995**, *102*, 1266.
(39) Olthof, E. H. T.; van der Avoird, A.; Wormer, P. E. S. *J. Chem. Phys.* **1996**, *105*, 8034. Olthof, E. H. T.; van der Avoird, A.; Wormer, P. E. S.; Liu, K.; Saykally, R. J. *J. Chem. Phys.* **1996**, *105*, 8051.
(40) Gregory, J. K.; Clary, D. C. *J. Phys. Chem.* **1996**, *100*, 18014.
(41) Gregory, J. K.; Clary, D. C. *J. Phys. Chem.* **1997**, *101*, 6813.
(42) Liu, K.; Cruzan, J. D.; Saykally, R. J. *Science* **1996**, *271*, 929 and references therein.
(43) Huisken, F.; Kaloudis, M.; Kulcke, A. *J. Chem. Phys.* **1996**, *104*, 17.
(44) Huisken, F. In *Molecular Complexes in the Earth's, Planetary, and Cometary Atmospheres*; Slanina, E., Vigasin, A. A., Eds.; World Scientific: Singapore, 1988; p 238.
(45) Liu, K.; Brown, M. G.; Carter, C.; Saykally, R. J.; Gregory, J. K.; Clary, D. C. *Nature* **1996**, *381*, 501.
(46) Liu, K.; Brown, M. G.; Saykally, R. J. *J. Phys. Chem.* **1997**, *101*, 8995.
(47) Pribble, R. N.; Zwier, T. S. *Science* **1994**, *265*, 75.
(48) Watanabe, T.; Ebata, T.; Tanabe, S.; Mikami, N. *J. Chem. Phys.* **1996**, *105*, 408.
(49) Schmitt, M.; Jacoby, C.; Roth, W.; Kleinermanns, K. *J. Phys. Chem. A* **1998**, *102*, 4471.
(50) Gruenloh, C. J.; Carney, J. R.; Arrington, C. A.; Zwier, T. S.; Fredericks, S. Y.; Jordan, K. D. *Science* **1997**, *276*, 1678.
(51) Buck, U.; Ettischer, I.; Melzer, M.; Buch, V.; Sadlej, J. *Phys. Rev. Lett.* **1998**, *80*, 2578.
(52) Roth, W.; Schmitt, M.; Jacoby, C.; Spangenberg, D.; Janzen, C.; Kleinermanns, K. *Chem. Phys.* **1998**, *239*, 1.
(53) Brudermann, J.; Melzer, M.; Buck, U.; Kazimirski, J.; Sadlej, J.; Buch, V. *J. Chem. Phys.*, in press.
(54) Rowland, B.; Kadagathur, S.; Devlin, J. P.; Buch, V.; Feldmann, T.; Wojcik, M. *J. Chem. Phys.* **1995**, *102*, 8328.
(55) Kim, K. S.; Mhin, B. J.; Choi, U. S.; Lee, K. *J. Chem. Phys.* **1992**, *97*, 6649. Kim, J.; Lee, J. Y.; Lee, S.; Mhin, B. J.; Kim, K. S. *J. Chem. Phys.* **1995**, *102*, 310.
(56) Clementi, E.; Corongiu, G.; Sciortino, F. *J. Mol. Struct.* **1993**, *296*, 205.
(57) Whalley, E.; Klug, D. D. *J. Chem. Phys.* **1986**, *84*, 78. Bertie, J. E.; Labbe, J.; Whalley, E. *J. Chem. Phys.* **1969**, *50*, 4501.
(58) McGraw, R.; Madden, W. G.; Bergen, M. S.; Rice, S. A.; Sceats, M. G. *J. Chem. Phys.* **1978**, *69*, 3483. Rice, S. A.; Bergen, M. S.; Belch, A. C.; Nielsen, G. *J. Phys. Chem.* **1983**, *87*, 4295.
(59) Wojcik, M.; Buch, V.; Devlin, J. P. *J. Chem. Phys.* **1993**, *99*, 2332.
(60) Hermansson, K.; Lingren, J.; Probst, M. M. *Chem. Phys. Lett.* **1995**, *233*, 371.
(61) Buch, V.; Sandler, P.; Sadlej, J. *J. Phys. Chem. B* **1998**, *102*, 8641.
(62) Kuwajima, S.; Warshel, A. *J. Phys. Chem.* **1990**, *94*, 460.
(63) Dunning, T. H. *J. Chem. Phys.* **1970**, *53*, 2823.
(64) Pedulla, J. M.; Vila, F.; Jordan, K. D. *J. Chem. Phys.* **1996**, *105*, 11091. Pedulla, J. M.; Kim, K.; Jordan, K. D. *Chem. Phys. Lett.* **1998**, *291*, 78.
(65) Hermansson, K.; Knuts, S.; Lingren, J. *J. Chem. Phys.* **1991**, *95*, 7486.
(66) Boys, S. F.; Bernardi, F. *Mol. Phys.* **1970**, *19*, 553.
(67) Turi, L.; Dannenberg, J. J. *J. Phys. Chem.* **1993**, *97*, 2488. Simon, S.; Duran M.; Dannenberg, J. J. *J. Chem. Phys.* **1996**, *105*, 11024.
(68) Cook, D. B.; Sordo, J. A.; Sordo, T. L. *Int. J. Quant. Chem.* **1993**, *48*, 375.
(69) Van Lenthe, J. H.; Vos, R. J.; van Duijneveldt-van de Rijdt, J. G. C. M.; Van Duijneveldt, F. B. *Chem. Phys. Lett.* **1998**, *143*, 435.
(70) Xanteas, S. S. *J. Chem. Phys.* **1996**, *104*, 8821.
(71) Szalewicz, K.; Jeziorski, B. *J. Chem. Phys.* **1998**, *109*, 1198.
(72) Frisch, M. J.; Trucks, G. W.; Schlegel, H. B.; Gill, P. M. W.; Johnson, B. G.; Robb, M. A.; Cheeseman, J. R.; Keith, T.; Petersson, G. A.; Montgomery, J. A.; Raghavachari, K.; Al-Laham, M. A.; Zakrzewski, V. G.; Ortiz, J. V.; Foresman, J. B.; Cioslowski, J.; Stefanov, B. B.; Nanayakkara, A.; Challacombe, M.; Peng, C. Y.; Ayala, P. Y.; Chen, W.; Wong, M. W.; Andres, J. L.; Replogle, E. S.; Gomperts, R.; Martin, R. L.; Fox, D. J.; Binkley, J. S.; Defrees, D. J.; Baker, J.; Stewart, J. P.; Head-Gordon, M.; Gonzalez, C.; Pople, J. A. Gaussian Inc.: Pittsburgh, PA, 1995.
(73) Devlin, J. P.; private communication; the analogous D_2O spectrum, together with the method to derive surface spectra of ice nanocrystals, can be found in Delzeit, L.; Devlin, J. P.; Buch, V. *J. Chem. Phys.* **1997**, *107*, 3726. The 90 K spectrum of the ice film in Figure 6 was also provided by Devlin, J. P.
(74) Walrafen, G. *J. Chem. Phys.* **1967**, *47*, 114.
(75) Stillinger, F. H. *Science* **1980**, *209*, 451.
(76) Buch, V. *J. Chem. Phys.* **1992**, *96*, 3814.
(77) Devlin, J. P. *Int. Rev. Phys. Chem.* **1990**, *9*, 29.
(78) Liu, S.; Bacic, Z.; Moskowitz, J. W.; Schmidt, K. E. *J. Chem. Phys.* **1994**, *101*, 10181.
(79) Sandler, P.; Sadlej, J.; Feldmann, T.; Buch, V. *J. Chem. Phys.* **1997**, *107*, 5022.
(80) Jackson, S. M.; Whitworth, R. W. *J. Chem. Phys.* **1995**, *103*, 7647. Jackson, S. M.; Nield, V. M.; Whitworth, R. W.; Oguro, M.; Wilson, C. C. *J. Phys. Chem.* **1997**, *101*, 6142. The proton-ordering transition is catalyzed by KOH doping of ice.
(81) Wilson, E. B.; Decius, J. C.; Cross, P. C. *Molecular Vibrations*; Dover: New York, 1980.
(82) Camy-Peyret, C.; Flaud, J. M. In *Molecular Spectroscopy: Modern Research*; (Nahari Rao, K., Ed.; Academic: London, 1985.
(83) Ikawa, I.; Maeda, S. *Spectrochim. Acta A*, **1968**, *24*, 655.
(84) Buch, V.; Devlin, J. P. *J. Chem. Phys.* **1999**, *110*, 3437.
(85) Sage, M. *Chem. Phys.* **1978**, *35*, 375.
(86) Scheid, F. *Numerical Analysis;* McGraw-Hill: New York, 1988.
(87) Reimers, J. R.; Watts, R. O. *Mol. Phys.* **1984**, *52*, 357 and references therein.
(88) The connection between the different Morse parameters is as follows: $\omega_i = \omega_e - 2\omega_e x_e$; $\omega_e = (2D_i\alpha_i^2/M_{OH})^{1/2}$; $\omega_e x_e = \alpha_i^2/(2M_{OH})$. A scaling parameter was defined $f = \omega_i/\omega_o$ (the subscript *o* denotes free OH). The rescaled Morse parameters of bond *i* were then calculated as $\alpha_i = \alpha_o f^{1/2}$; $\omega_e = \omega_i' + 2\omega_e x_e$; $D_i = (\omega_e/\alpha_i)^2 M_{OH}/2$.
(89) Buch, V. *J. Chem. Phys.* **1992**, *97*, 726.
(90) Anderson, J. B. *J. Chem. Phys.* **1975**, *63*, 1499; **1976**, *65*, 4121.
(91) Hernandez, J.; Uras, N.; Devlin, J. P. *J. Chem. Phys.* **1998**, *108*, 4525.
(92) The minimum dimer energy calculated with EMP(fl) is −5.54 kcal/mol, and with EMP(r), −5.476 kcal/mol. On the basis of analysis of ab initio results, Mas, E. M.; Szalewicz, K., *J. Chem. Phys.* **1996**, *104*, 7606, suggested a dimer well depth of 5.1−0.1 kcal/mol.
(93) Gregory, J. K.; Clary, D. C.; Liu, K.; Brown, M. G.; Saykally, R. J. *Science* **1997**, *275*, 814.
(94) Hobbs, P. V. *Ice Physics*; Clarendon: Oxford, 1974.
(95) The minimum energies of the different D_{bfl} isomers are nearly equal; however, the cluster dipoles at the minima differ substantially (2.65 and 3.05 Debye for trans and cis, in EMP(r)).
(96) The dangling OH of the DA molecule in H_{nxt} was found to perform a similar motion as in the nonamers; however, here the second minimum is higher in energy by 0.4 kcal/mol, and the probability to visit that minimum by a replica in a DMC simulation is only about 20%.
(97) Tsai, C. J.; Jordan, K. D. *J. Chem. Phys.* **1993**, *99*, 6957.
(98) McDonald, S.; Ojamäe, L.; Singer, S. J. *J. Phys. Chem. A* **1998**, *102*, 2824.
(99) Buck, U.; Meyer, H. *J. Chem. Phys.* **1986**, *84*, 4854.
(100) Buck, U. *J. Phys. Chem.* **1994**, *98*, 5190.
(101) Brudermann, J.; Buch, V.; Buck, U.; Gerber, R. B.; Krohne, R.; Lohbrandt, P. In *Structure and Dynamics of Clusters*; Kondow, T., Kaya, K., Terasaki, A., Eds.; Universal Academic: Tokio, 1996; p 45.
(102) Buck, U. *Adv. At. Mol. Opt. Phys.* **1995**, *35*, 121.